CO_2 LASER PULSING TECHNIQUES
FINAL REPORT

APRIL 1972

NORTHROP CORPORATION

LASER SYSTEMS DEPARTMENT
3401 West Broadway
Hawthorne, California 90250

CO_2 LASER PULSING TECHNIQUES
FINAL REPORT

APRIL 1972

Office of Naval Research
Contract No. N00014-70-C-0185
December 1969 to February 1972

Prepared by
D. B. Cohn, R. G. Eguchi
W. B. Lacina, W. H. Steier, M. M. Mann

Sponsored by
ADVANCED RESEARCH PROJECTS AGENCY
Order No. 306

Principal Investigator: Dr. M. M. Mann
Tel: (213) 675-4611

NORTHROP CORPORATION
Laser Systems Department
3401 West Broadway
Hawthorne, California 90250

UNCLASSIFIED

Security Classification

DOCUMENT CONTROL DATA - R & D

(Security classification of title, body of abstract and indexing annotation must be entered when the overall report is classified)

1. ORIGINATING ACTIVITY *(Corporate author)*
NORTHROP CORPORATION
Laser Systems Department
3401 W. Broadway, Hawthorne, Calif. 90250

2a. REPORT SECURITY CLASSIFICATION
Unclassified

2b. GROUP
-

3. REPORT TITLE

CO_2 LASER PULSING TECHNIQUES, FINAL REPORT

4. DESCRIPTIVE NOTES *(Type of report and inclusive dates)*
FINAL REPORT, December 1969 to February 1972

5. AUTHOR(S) *(First name, middle initial, last name)*
D. B. Cohn, R. G. Eguchi, W. B. Lacina, W. H. Steier, M. M. Mann

6. REPORT DATE	7a. TOTAL NO. OF PAGES	7b. NO. OF REFS
April 1972	57	29

8a. CONTRACT OR GRANT NO.	9a. ORIGINATOR'S REPORT NUMBER(S)
N00014-70-C-0185	NLSD 72-9R
b. PROJECT NO. 306	
c.	9b. OTHER REPORT NO(S) *(Any other numbers that may be assigned this report)*
d.	-

10. DISTRIBUTION STATEMENT
none

11. SUPPLEMENTARY NOTES	12. SPONSORING MILITARY ACTIVITY
none	Office of Naval Research Department of the Navy Arlington, Virginia 22217

13. ABSTRACT

This is the final report of a program to study "CO_2 Laser Pulsing Techniques," sponsored by the Advanced Research Project Agency, under Office of Naval Research Contract N00014-70-C-0185. Stable mode-locking and pulse coupling of a longitudinal discharge CO_2 laser, using a single electrooptic element, was demonstrated successfully. The experimental results and data on the effect of modulator detuning and coupling factor variations are presented. Similar experiments were performed with a CO_2 TEA laser in which loss-locking was obtained using the internal electrooptic element as an AM modulator. However, attempts at phase-locking were unsuccessful. Results of a detailed investigation of the discharge properties of the TEA laser are presented. The processes involved in mode-locking and their bearing on the observed results are discussed.

DD FORM 1 NOV 65 1473

ib

UNCLASSIFIED

Security Classification

14 KEY WORDS	LINK A		LINK B		LINK C	
	ROLE	WT	ROLE	WT	ROLE	WT
MODE-LOCKING						
PULSE COUPLING						
ELECTROOPTIC MODULATOR						
CO_2 LASERS						
TEA LASERS						

NOTICE

The views and conclusions contained in this document are those of the authors and should not be interpreted as necessarily representing the official policies, either expressed or implied, of the Advanced Research Projects Agency or the U. S. Government.

id

TABLE OF CONTENTS

1.0 INTRODUCTION

The objective of this program was to investigate CO_2 laser pulsing techniques. The effort was directed at developing techniques for generating pulse trains with high amplitude and temporal stability. In addition, techniques for efficiently modulating the resulting pulse trains were investigated.

This is the final report on the effort and contains a review of the results of the experimental investigation of mode-locking and pulse coupling using internal electrooptic elements. Parts of this work have been previously reported.[1,2,3] Loss and phase locking of both conventional low pressure longitudinal discharge lasers and TEA type lasers were investigated. The modulator configuration and its operation is discussed in Section 2.0 of this report.

Very low modulator drive power ($\sim$1 mW) was required to obtain locking of a low pressure conventional CO_2 laser. Therefore, it was possible to obtain stable locking by driving the modulator with a stable, low power, rf oscillator. The typical mode-locked output consisted of 20 ns pulses with a 7 MHz repetition rate. In addition, simultaneous mode-locking and pulse coupling using a single internal electrooptic element was achieved. This makes it possible to pulse dump or modulate without the additional losses and optical complexity associated with a separate modulator. The effects of modulator detuning and coupling factor variation were also investigated. These results are reviewed in Section 3.0.

Experiments were performed with TEA lasers to exploit the pressure broadened line width and obtain narrower pulses and higher pulse repetition rates. It was possible to loss-lock this laser using the internal electrooptic element as an AM modulator. However, attempts at phase-locking were unsuccessful. A detailed investigation of the discharge properties of a number of TEA discharge configurations was undertaken to explain the observed behavior. The results of these diagnostic measurements as well as the mode locking experiments are discussed in Section 4.0.

In Section 5.0, the processes involved in self mode-locking, loss mode-locking, and phase mode-locking are discussed and a qualitative explanation is presented for the observed results.

2.0 MODULATOR CONFIGURATION AND CHARACTERISTICS.

An externally applied electric field can induce a birefringence in the optical refractive index of a crystalline medium. For a crystal lacking inversion symmetry, this is the linear electrooptic effect, and the change in refractive index is proportional to the applied field. An induced birefringence will lead to phase retardations and/or elliptical polarization of a light beam propagating through the medium, and thus, the electrooptic effect can be exploited for a wide variety of optical modulation, mode-locking, and pulse dumping schemes. Ideally, the electrooptic modulator material should have high electrical resistivity, large nonlinear coefficients, small absorption losses, and a high refractive index. Furthermore, since the birefringence induced in the refractive index (per unit field strength) is typically very small, long crystals of good optical quality are usually necessary in order to produce adequate phase retardations. GaAs was employed in these experiments since it has a high damage threshold and large high resistivity single crystals were readily available commercially.

The basic theory of the electrooptic effect, specialized to GaAs and the experimental geometry will be described here.

The nonlinear polarization $\vec{P}^{NL}(\omega_2 = \omega_1 + \omega_o)$ induced by the interaction of two electric fields $\vec{E}(\omega_1)$ and $\vec{\mathcal{E}}(\omega_o)$ is given by

$$P_i^{NL}(\omega_2) = d_{ijk}(\omega_2, \omega_1, \omega_o)\, E_j(\omega_1) \mathcal{E}_k(\omega_o), \qquad (2.1)$$

where, for GaAs, the susceptibility tensor $\tilde{d}$ has components which vanish unless (ijk) is a permutation of (xyz). All non-zero coefficients have the

value $d = 1.85 \times 10^{-7}$ esu, and can be assumed to be independent of ω. Thus,

$$P_x^{NL}(\omega_2) = dE_y(\omega_1)\ \mathcal{E}_z(\omega_o) + dE_z(\omega_1)\ \mathcal{E}_y(\omega_o)$$

$$P_y^{NL}(\omega_2) = dE_z(\omega_1)\ \mathcal{E}_x(\omega_o) + dE_x(\omega_1)\ \mathcal{E}_z(\omega_o) \qquad (2.2)$$

$$P_z^{NL}(\omega_2) = dE_x(\omega_1)\ \mathcal{E}_y(\omega_o) + dE_y(\omega_1)\ \mathcal{E}_x(\omega_o)\ .$$

If $\vec{\mathcal{E}}(\omega_o)$ represents an applied modulation field, and $\vec{E}(\omega_1)$ an optical field then a nonlinear polarization at an optical frequency $\omega_2 = \omega_1 + \omega_o$ will be induced. Assume that ω_o is chosen to be the axial-mode frequency separation of two simultaneously oscillating laser cavity modes of equal amplitude, with frequencies ω_1 and ω_2:

$$\vec{E}(\omega_1) = \vec{E} \exp(i\omega_1 t)$$

$$\vec{E}(\omega_2) = \vec{E} \exp(i\omega_2 t) \qquad (2.3)$$

Then an effective dielectric tensor for ω_2 that accounts for both linear dispersion and the nonlinear electrooptic effect would be given by

$$\tilde{\epsilon}_{eff}(\omega_2) = \tilde{\epsilon}_o + 4\pi d \begin{pmatrix} 0 & \mathcal{E}_z & \mathcal{E}_y \\ \mathcal{E}_z & 0 & \mathcal{E}_x \\ \mathcal{E}_y & \mathcal{E}_x & 0 \end{pmatrix} \qquad (2.4)$$

and similarly for ω_1. The unperturbed dielectric tensor $\tilde{\epsilon}_o$ is just a constant, $\epsilon_o(\tilde{1})$, and will be assumed to be independent of the frequency ω.

The eigenvectors of $(\tilde{1} - \hat{k}\hat{k}) \cdot \tilde{\epsilon}^{-1}(\omega)$ determine the polarization directions of the optical modes which can propagate in the crystal, and the corresponding eigenvalues are the values of $1/n^2$. Thus, since d is small,

$$\tilde{\epsilon}^{-1}_{eff} \simeq \epsilon_o^{-1} \left\{ 1 - (4\pi d/\epsilon_o) \begin{pmatrix} 0 & \mathcal{E}_z & \mathcal{E}_y \\ \mathcal{E}_z & 0 & \mathcal{E}_x \\ \mathcal{E}_y & \mathcal{E}_x & 0 \end{pmatrix} \right\} \tag{2.5}$$

Consider a crystal of GaAs oriented so that the cavity-mode fields $\vec{E}(\omega_1)$ and $\vec{E}(\omega_2)$ are polarized along (110), with a propagation direction along $(1\bar{1}0)$, and with an applied field $\vec{\mathcal{E}}(\omega_o)$ in the (001) direction. Then

$$\tilde{\epsilon}^{-1}_{eff} \simeq \epsilon_o^{-1} \left\{ \tilde{1} - (4\pi d\, \mathcal{E}/\epsilon_o) \begin{pmatrix} 0 & 1 & 0 \\ 1 & 0 & 0 \\ 0 & 0 & 0 \end{pmatrix} \right\} \tag{2.6}$$

and this tensor has eigenvectors (110), $(1\bar{1}0)$, and (001). Since these are also eigenvectors of $(\tilde{1} - \hat{k}\hat{k})$, they are eigenvectors of $(\tilde{1} - \hat{k}\hat{k}) \cdot \tilde{\epsilon}^{-1}(\omega)$, with corresponding eigenvalues:

$$\begin{aligned} 1/n_1^2 &= \epsilon_o^{-1} (1 - 4\pi d\, \mathcal{E}/\epsilon_o) \\ 1/n_2^2 &= \epsilon_o^{-1} (1 + 4\pi d\, \mathcal{E}/\epsilon_o) \\ 1/n_3^2 &= \epsilon_o^{-1} \end{aligned} \tag{2.7}$$

Since the cavity modes were initially assumed to be polarized along (110), the effect of the driving field $\vec{\mathcal{E}}(\omega_o)$ is to phase modulate the optical fields, but not to introduce elliptical polarization, since (110) still remains an eigenmode for propagation with $n^2 = (\epsilon_o + 4\pi d\,\mathcal{E})$. Thus, a field applied on (001) with a frequency ω_o tuned to the axial mode separation can be used to lock cavity modes polarized along (110) by intracavity phase perturbation, and it will not rotate the plane of polarization.

Next, suppose the field $\vec{\mathcal{E}}_o$ is a dc field applied along (110). Then the effective dielectric tensor for the cavity modes (at frequency ω_1 or ω_2) is

$$\tilde{\epsilon}_{eff} = \tilde{\epsilon}_o + (4\pi d\,\mathcal{E}_o/\sqrt{2}) \begin{pmatrix} 0 & 0 & 1 \\ 0 & 0 & 1 \\ 1 & 1 & 0 \end{pmatrix}. \qquad (2.8)$$

The eigenvectors of $(\tilde{1} - \hat{k}\hat{k}) \cdot \tilde{\epsilon}^{-1}_{eff}(\omega)$, with the corresponding eigenvalues for refractive index, are easily shown to be

$$\begin{aligned} \hat{e}_1 &= (1/2,\ 1/2,\ 1/\sqrt{2}) & n_1^2 &= \epsilon_o + 4\pi d\,\mathcal{E}_o \\ \hat{e}_2 &= (1/2,\ 1/2,\ -1/\sqrt{2}) & n_2^2 &= \epsilon_o - 4\pi d\,\mathcal{E}_o \end{aligned} \qquad (2.9)$$

As shown in Figure A.1 the application of a field $\mathcal{E}_o$ along (110) results in a new set of eigenmodes rotated 45^o from the crystal directions (001)

Figure 2.1. Pulse Dumping Configuration.

and (110). Thus, for cavity modes polarized along (110), there will be an elliptical polarization produced by the field $\vec{e}_o$. That is, the original cavity modes $\vec{E}(\omega)$ can be decomposed into two components referred to the new set of polarization modes $\hat{e}_1$, $\hat{e}_2$, and each of these components will propagate with different phase velocities in the crystal. This results in an elliptically polarized optical field. The amplitude of the component of the field polarized orthogonal to the input will depend upon the length of the crystal and the magnitude of the applied field. If the optical field propagating in the crystal is written as

$$\vec{E}(\vec{r}, t) = (E\, e^{-i\omega t}/\sqrt{2})\,[\hat{e}_1\, e^{i\vec{k}_1 \cdot \vec{r}} + \hat{e}_2\, e^{i\vec{k}_2 \cdot \vec{r}}], \tag{2.10}$$

then $\vec{E}(0, t)$ will be initially polarized along (110). Since $|\vec{k}_1| = n_1\, \omega/c$, $|\vec{k}_2| = n_2\, \omega/c$, we have $(\vec{k}_1 + \vec{k}_2) = 2\vec{k}$, and the field $\vec{E}(\vec{r}, t)$ can be written more simply as

$$\vec{E}(\vec{r}, t) = (E/\sqrt{2})\, \exp\,[\, -i\omega t + i\vec{k} \cdot \vec{r}\,]\, x$$

$$[\hat{e}_1\, \exp\,(i\Delta\vec{k} \cdot \vec{r}/2) + \hat{e}_2\, \exp\,(-i\Delta\vec{k} \cdot \vec{r}/2)], \tag{2.11}$$

where $\Delta\vec{k} = \vec{k}_1 - \vec{k}_2$. Thus, it is sufficient to consider only the amplitude of the wave as it travels through the crystal, and suppress the phase factor $\exp\,(-i\omega t + i\vec{k} \cdot \vec{r})$:

$$\vec{E}(\vec{r}\,) = (E/\sqrt{2})\,[\,\hat{e}_1\, \exp\,(i\Delta\vec{k} \cdot \vec{r}/2) + \hat{e}_2\, \exp\,(-i\Delta\vec{k} \cdot \vec{r}/2)]\,. \tag{2.12}$$

At any distance $\vec{r}$ in the medium, the component of the field $\vec{E}(\vec{r}\,)$ along (110) is given by

$$E \cos\varphi = \vec{E} \cdot (\hat{e}_1 + \hat{e}_2)/\sqrt{2} = E \cos\,(\Delta\vec{k} \cdot \vec{r}/2), \tag{2.13}$$

so that the angle φ can be expressed as

$$\varphi = \vec{\Delta k} \cdot \vec{r}/2 = \omega \ell \Delta n/2c, \qquad (2.14)$$

where $\Delta n = \left| n_1 - n_2 \right| = 4\pi d\, \mathcal{E}_o / n_o$. If the static field $\mathcal{E}_o$ is denoted by $\mathcal{E}_o = V_o/t$, where V_o is the applied voltage and t the crystal thickness, then

$$\varphi = \pi \ell V_o n_o^3 r_{41}/(2\, \lambda_o t) \qquad (2.15)$$

where the electrooptic coefficient $r_{41} = 8\pi d/n_o^4$ has been introduced, and λ_o is the free-space wavelength. Thus, if a polarization selector such as Brewster-plate is used to couple out a pulse which has made a double pass through a crystal of length, ℓ, the total reflected power is, apart from geometric factors, proportional to $\sin^2(2\varphi)$.

We have successfully demonstrated that it is possible to simultaneously mode-lock the CO_2 laser by intracavity phase perturbation, and to output couple the pulses by polarization dumping. The technique employs a GaAs modulator with two sets of electrodes: a field of frequency ω_o is applied along (001), and mode-locked pulses are coupled out by a dc pulsed field applied along (110). The geometry of the modulator is shown in the inset of Figure 3.1. The fractional power that is coupled out by reflection at the Brewster plate of index n is

$$P_{out}/P_o = \left(\frac{n^2 - 1}{n^2 + 1} \right)^2 \sin^2 (2\varphi). \qquad (2.16)$$

The experimental set-up and the results of measurements are described in the next section for a low pressure cw CO_2 laser.

3.0 LOW PRESSURE CW CO_2 LASER EXPERIMENTS

Previous approaches to mode-locking of the CO_2 laser have depended on loss modulation[4-6] or nonlinear interaction in the gain medium[7-8]. In experiments reported here, mode-locking was obtained with the use of an intracavity electrooptic phase modulator driven at frequencies near the axial-mode interval. Drive requirements were minimized and locking stability was enhanced by resonating the modulator crystal at the drive frequency.

The laser configuration employed in these experiments consisted of a 40-mm-i.d. x 6-m discharge tube in a 22-m folded optical resonator, providing an axial-mode separation of 6.8 MHz (Figure 3.1). All components were mounted on massive granite supports to provide mechanical stability. The resonator configuration and mirror focal lengths were chosen with the aid of a resonator design computer program to simultaneously satisfy the requirements for a large mode volume in the discharge region and a small beam diameter (~1 mm) at the output end of the resonator where the modulator element was located. A variable aperture was included in the cavity to provide transverse-mode selection. A slow-speed chopper was interposed in the optical path to limit the duty cycle to approximately 0.5% in order to minimize the possibility of thermal damage to the modulator element or output mirror. The aperture time was sufficiently great (200 μsec to 2 sec) to insure that conditions were characteristic of cw operation. The laser output from a 2% transmitting output mirror was monitored with a liquid-helium-cooled Ge:Cu detector.

A high-resistivity GaAs crystal, 3 x 3 x 50 mm, with electrodes deposited on the (001) faces, was used as the phase modulator. The optical field was polarized along the (110) direction by a sodium chloride Brewster window

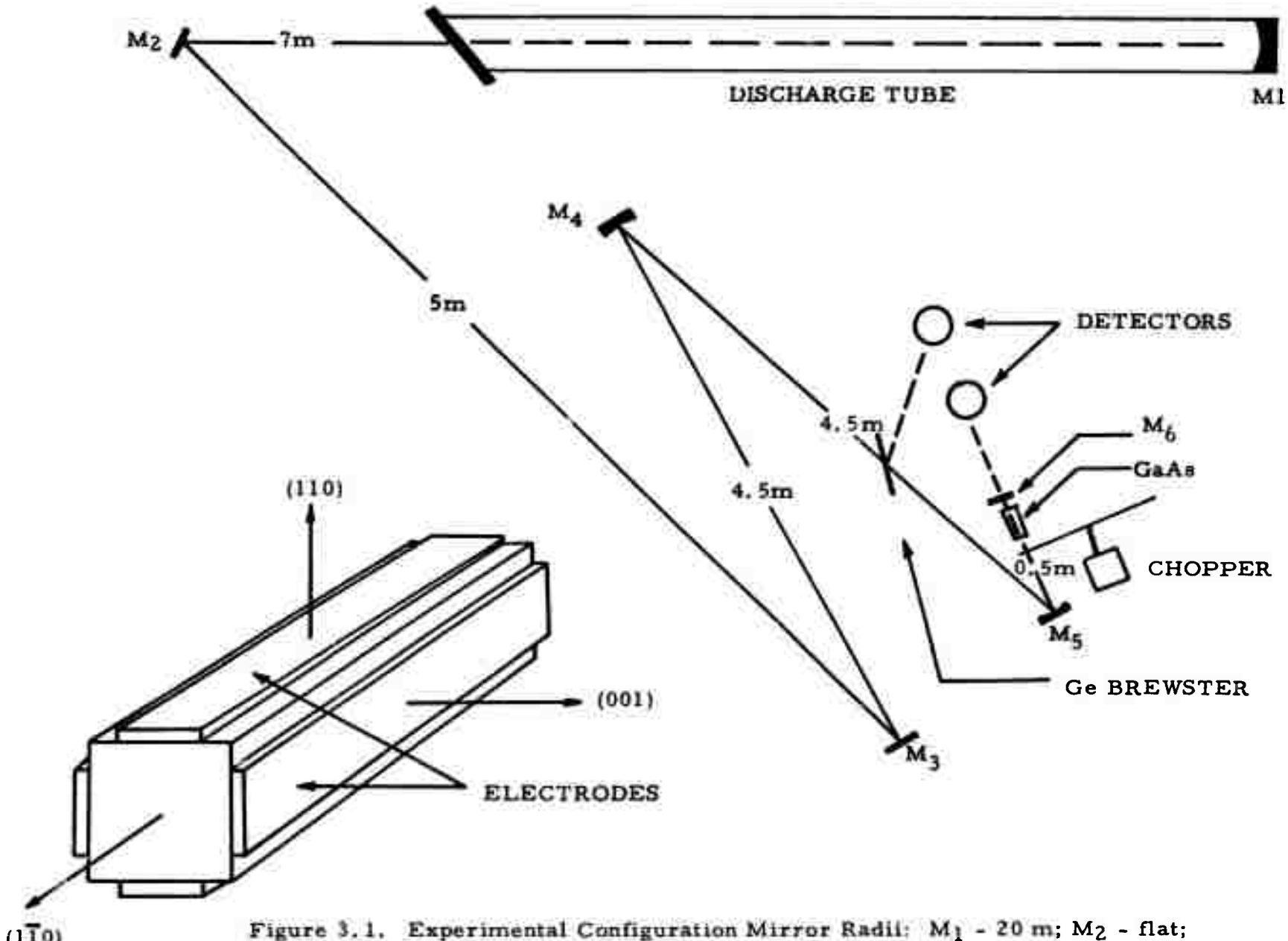

Figure 3.1. Experimental Configuration Mirror Radii: M_1 - 20 m; M_2 - flat; M_3 - flat; M_4 - 10 m; M_5 - 1 m; M_6 - flat.

on the discharge tube. The crystal was resonated in a high Q (~300) parallel LC circuit at a frequency corresponding to the drive frequency. The modulator resonator was inductively coupled to a tunable rf driver. Under typical operating condition, a 10-torr mixture of CO_2 (4.5%): N_2 (12.0%): He (83.5%) was used. The discharge current was 20 mA.

With the rf driver tuned to the fundamental axial-mode frequency, stable locking could be obtained with a signal as small as 0.5V peak-to-peak from the modulator driver. This corresponds to a modulator drive power of 1 mW. Under these conditions, pulses with Gaussian profiles 40 nsec wide and 147 nsec period were observed. Increasing the signal to 10 V peak-to-peak decreased the pulse duration to 25 nsec (Figures 3.2 and 3.3). Further increases in the applied voltage produced a gradual sharpening of the pulse form, but quantitative measurements were hampered by the bandwidth limitations of the detection electronics. The ratio of peak mode-locked pulse power to cw power was 4.5 to 5.5. The average power in the locked mode of operation was 94% of the cw power. These results are consistent with the observations of the rf spectral characteristics of the detector output which indicated that five to six modes were locked.

Measurements were made of the phase of the optical pulses relative to the modulator drive signal as a function of modulator detuning. Detuning was determined by simultaneously observing the modulation signal and the axial mode beat frequency spectrum appearing on the detector output on an rf spectrum analyzer. Zero detuning was defined as the point at which the modulation frequency coincided with the dominant free running axial mode beat frequency. With zero detuning the pulses traversed the crystal at either (or both) extremum(a) of the phase perturbation, depending on the critical positioning of the output mirror. The three cases are illustrated

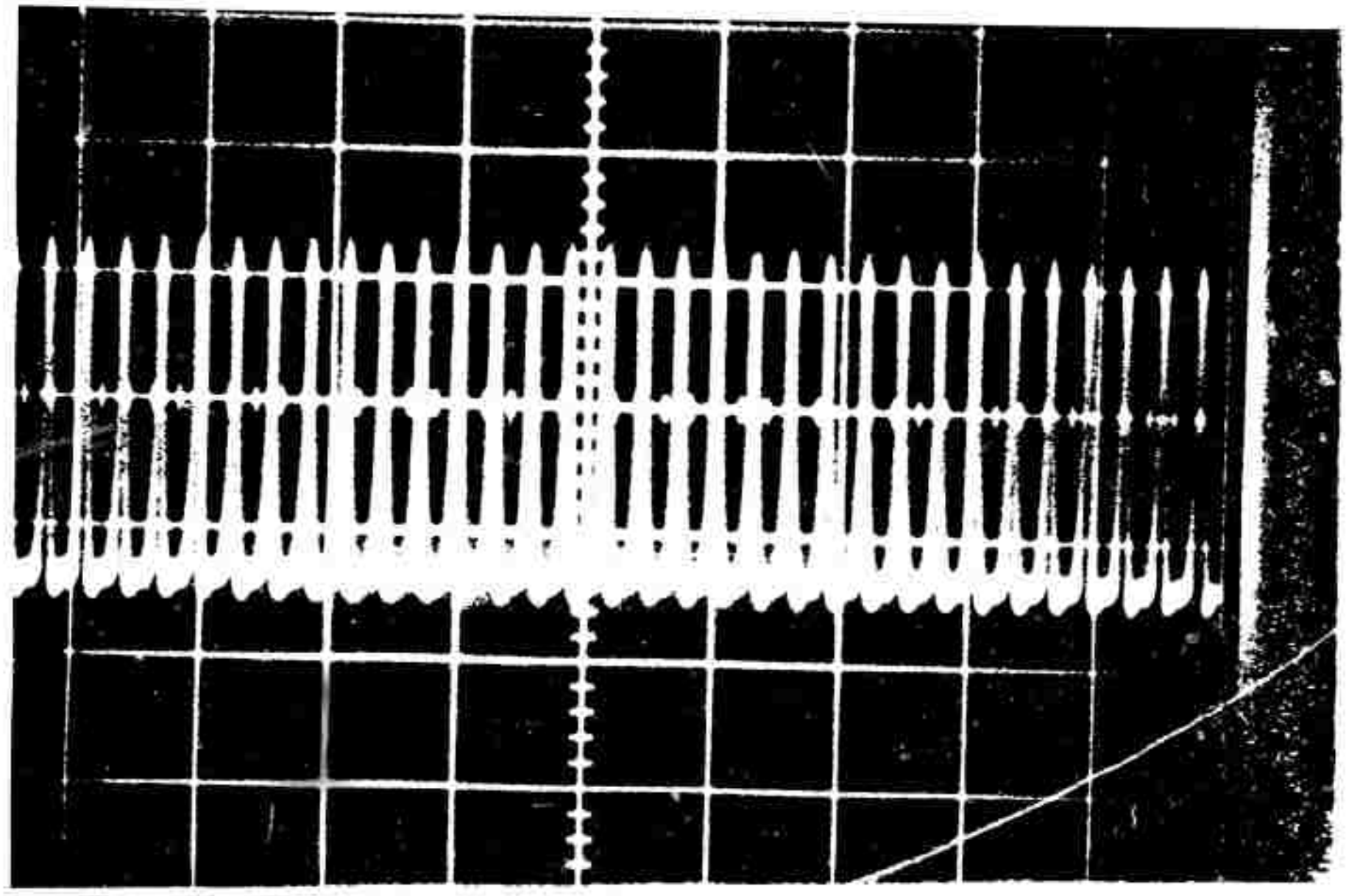

Figure 3.2. Mode-Locked Pulse Train - 0.5 V Drive (Horizontal Scale 500 ns)

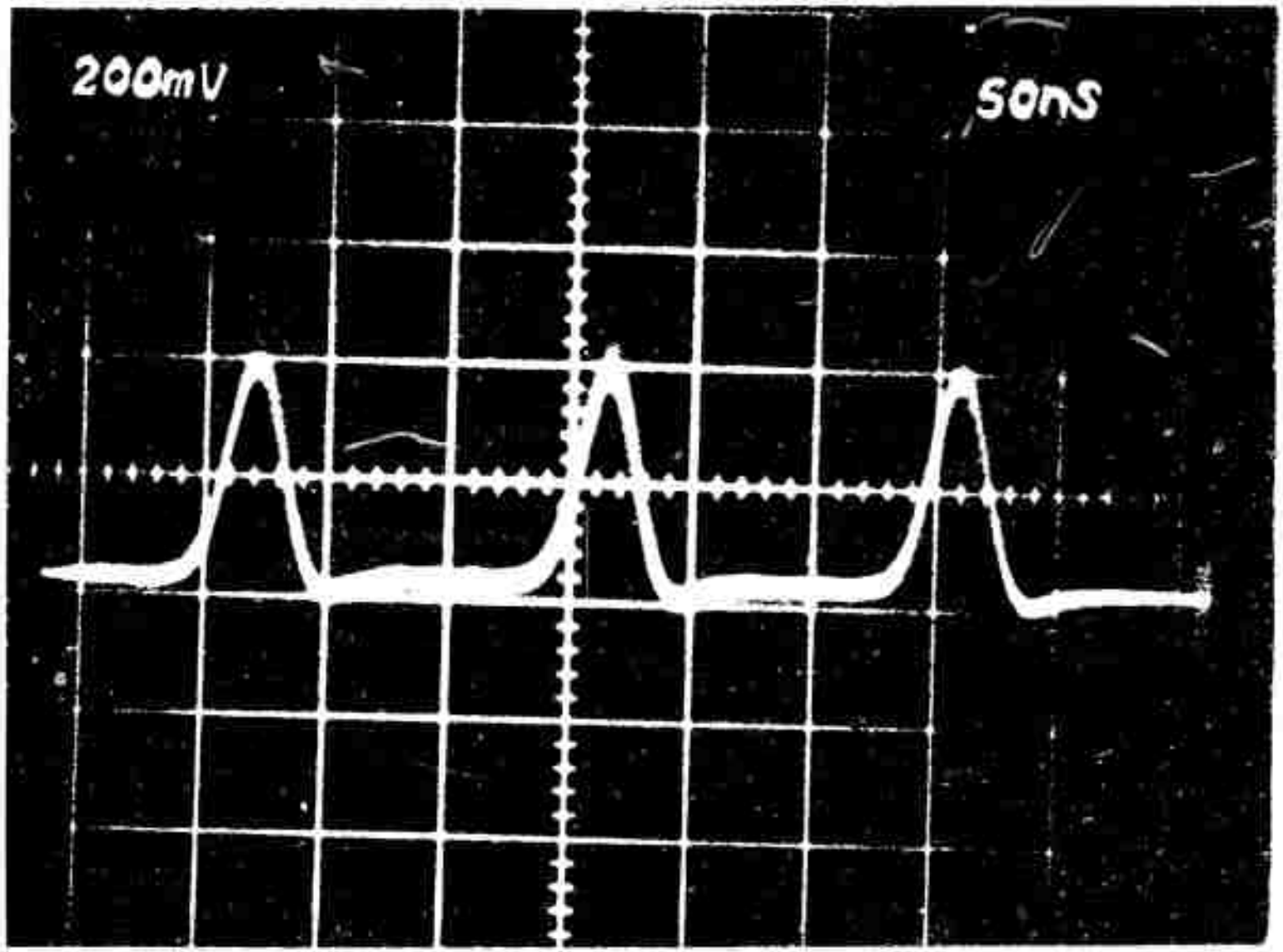

Figure 3.3. Mode-Locked Pulse Train - 10 V Drive

in Figure 3.4. In each instance the upper trace is the drive signal and the lower trace is the laser output. In these figures all extraneous delays have been compensated, and the modulator driver was tuned to the axial-mode interval. The repetition rate of the pulse train in the lower figure is equal to twice the fundamental mode frequency.

The effect of detuning is presented in Figure 3.5 and 3.6 which show the effect of positive or negative detuning, respectively. The strong asymmetry in the tuning characteristic is evident from these figures. Stable locking could be induced when the modulation frequency was within a range of -75kHz to +170kHz of the fundamental axial-mode frequency of 6.8 MHz. In each case the modulator resonator was tuned to the drive frequency. The drive voltage required to obtain locking at the extremes of the tuning range was approximately 20 times as great as that required for zero detuning. Quantitative comparison between the experiment and theory have not been made, but the results are in qualitative agreement with both theory [9, 10] and previous experimental work on the He-Ne lasers [11].

Simultaneous mode-locking and pulse coupling of a CO_2 laser has also been achieved using a single internal GaAs element with electrodes on both the (001) and (110) faces. The experimental configuration was basically the same as that used for the mode-locking experiments described above. A 3 x 3 x 50 mm GaAs crystal with electrodes deposited on the (001) and (110) faces and AR coatings on the $(1\bar{1}0)$ faces (see inset, Figure 3.1), was used both for locking and coupling. In the absence of a coupling signal, the optical field was polarized along the (110) direction.

A signal at the axial-mode difference frequency with an amplitude of approximately 10-V peak-to-peak was applied across the (001) faces to

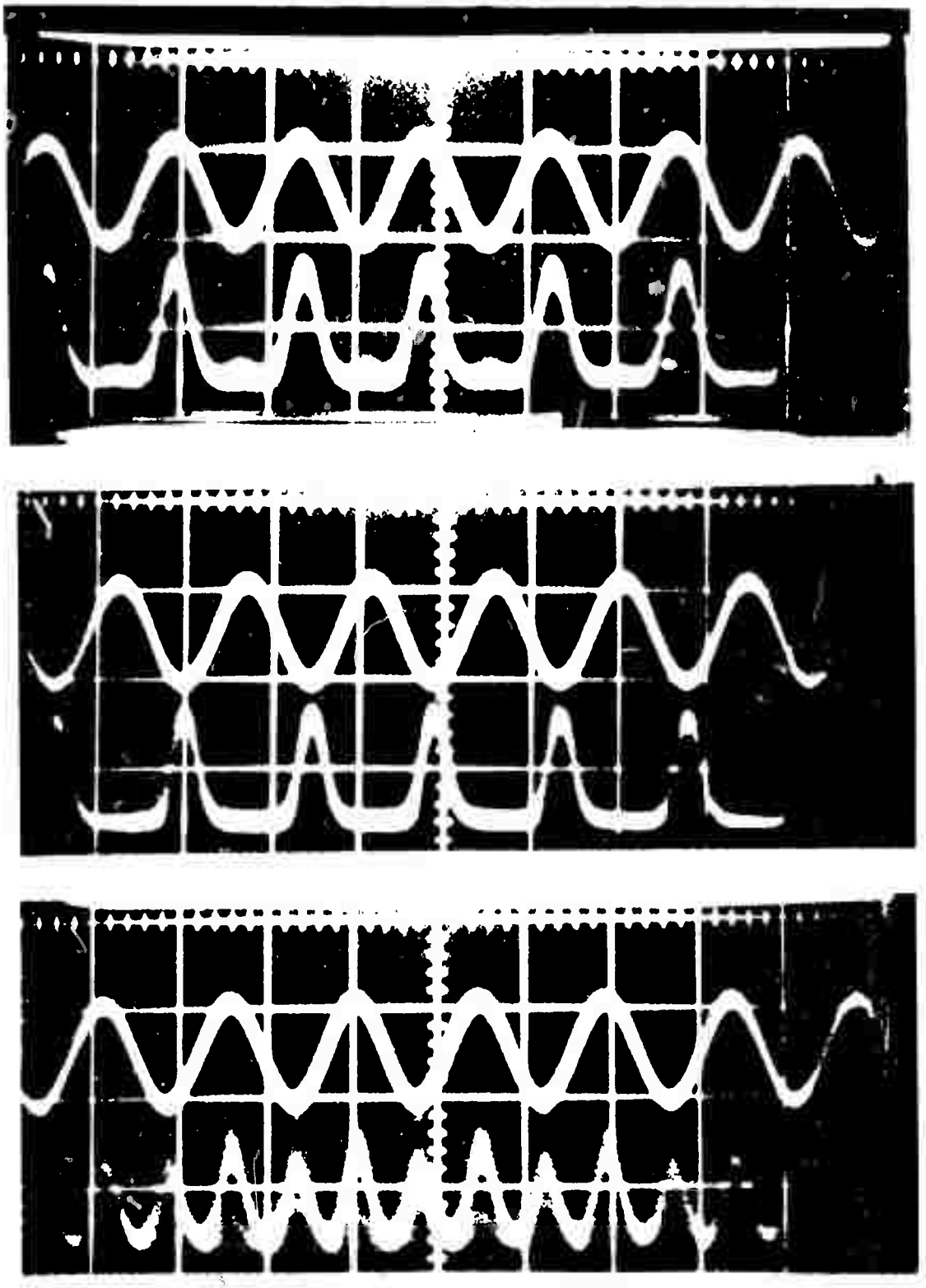

Figure 3.4. Relative phase of mode-locked pulse and modulator drive signal for zero detuning.

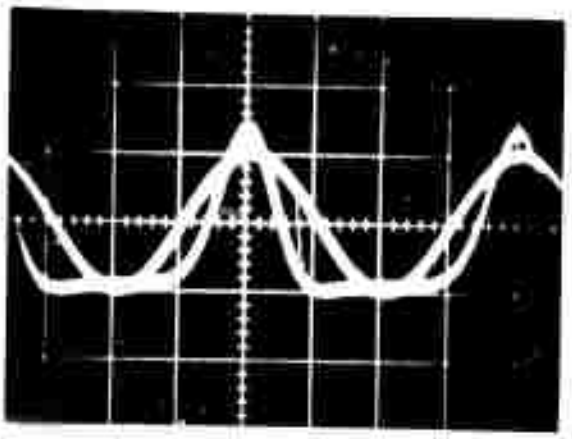

6.78 MHz

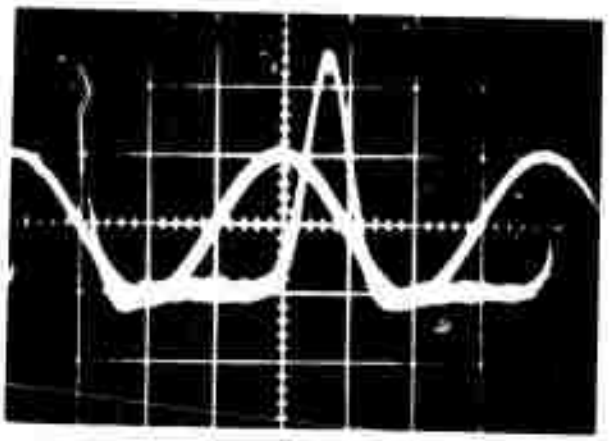

6.86 MHz

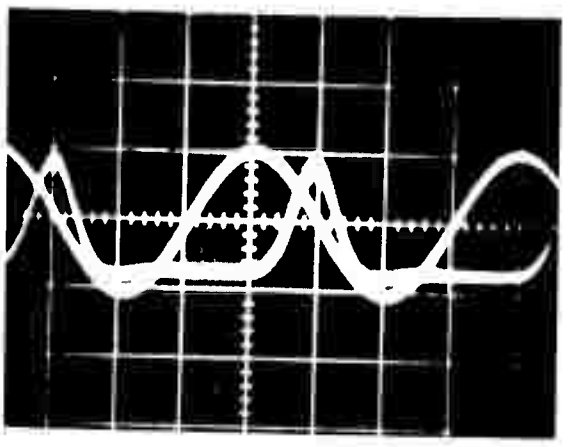

6.90 MHz

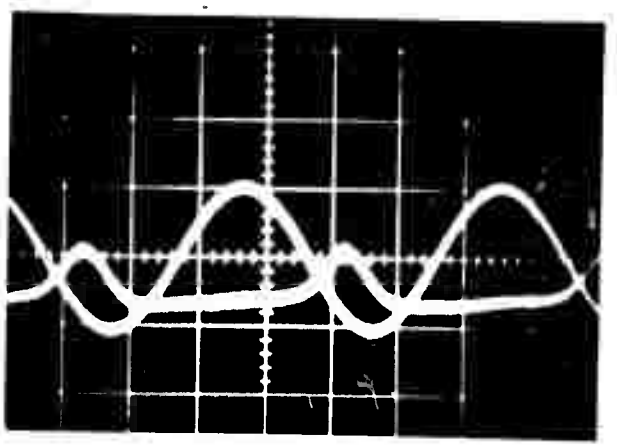

6.97 MHz

Figure 3.5. Relative phase of mode-locked pulse and modulator drive signal for positive detuning.

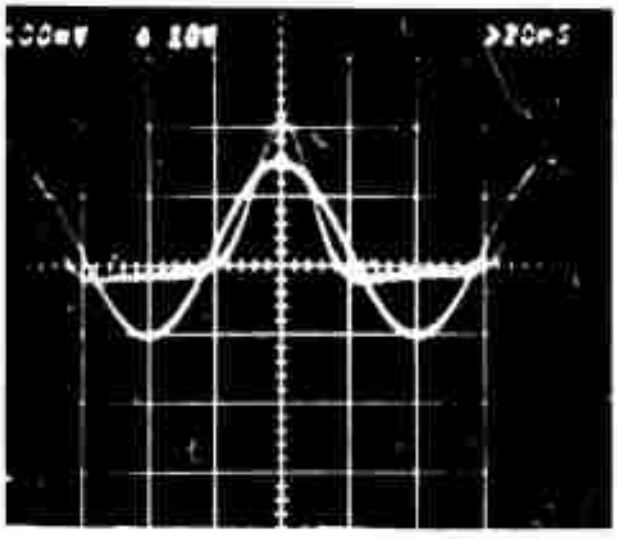

6.80 mHz

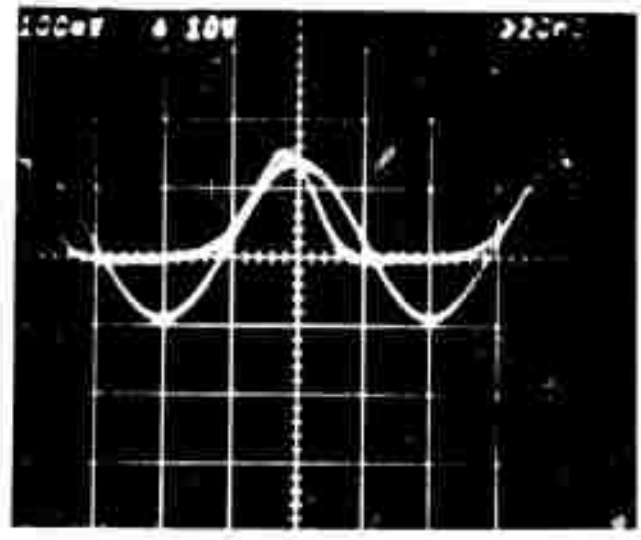

6.775 mHz

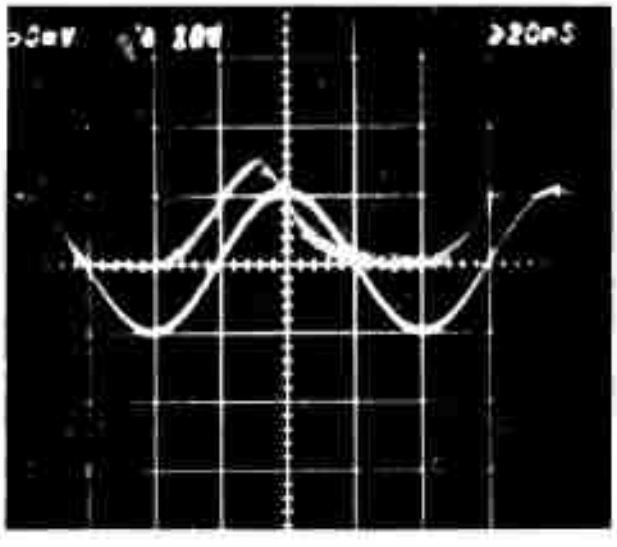

6.750 mHz

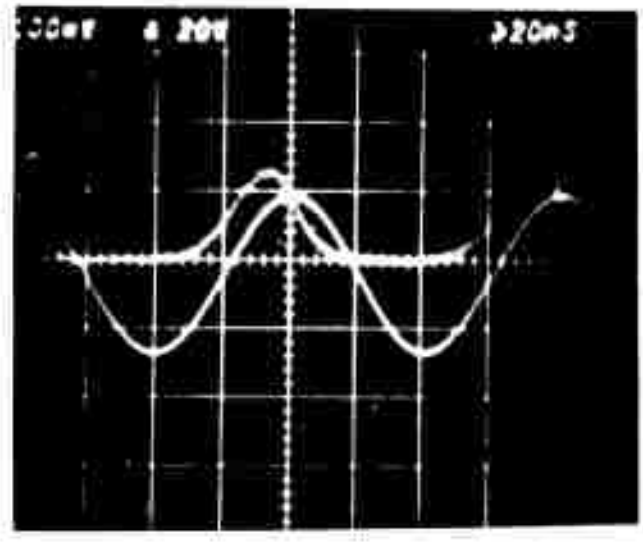

6.725 mHz

Figure 3.6. Relative phase of mode-locked pulse and modulator drive signal for negative detuning.

produce phase-locking of the axial modes. Coupling of selected laser pulse(s) was effected by applying a voltage pulse on the (110) faces to induce a birefringence in the GaAs crystal, as described in Section 2. The resultant optical component polarized along (001) was coupled out of the resonator by a polarization analyzer in the form of a germanium flat oriented at the Brewster angle. (The NaCl Brewster on the discharge tube provided insufficient polarization discrimination for this purpose).

Liquid-nitrogen-cooled Ge:Au detectors were employed, and power measurements were made with a calibrated thermopile. Peak intra-cavity pulse power in mode-locked operation was 2 kW.

Figure 3.7 shows typical results. The coupling voltage pulse is displayed in the upper trace, the mode-locked pulse train observed through M_6 (see Figure 3.1) is displayed in the center trace, and the coupled output pulse is shown in the lower trace. It should be noted that the center trace is delayed by one pulse period with respect to the lower trace, since it is necessary for the mode-locked pulse to complete a round trip in the resonator before being observed at M_6. The coupling voltage pulse in this case had an amplitude of 440 V, and the measured cavity coupling coefficient was $2.5 \pm 0.5\%$. The theoretical value corresponding to this voltage was 3.7% (Figure 3.8), assuming a uniform modulating field in the crystal, and taking account of the reflectivity of the germanium Brewster plate. The difference between the experimental and theoretical values is attributable to the field distortion produced by the presence of the orthogonal set of electrodes. This conclusion is supported by the fact that it was possible to obtain coupling factors in excess of the predicted values by displacing the modulator element so the beam passed through the crystal near one of the corners where the field assumed its highest values.

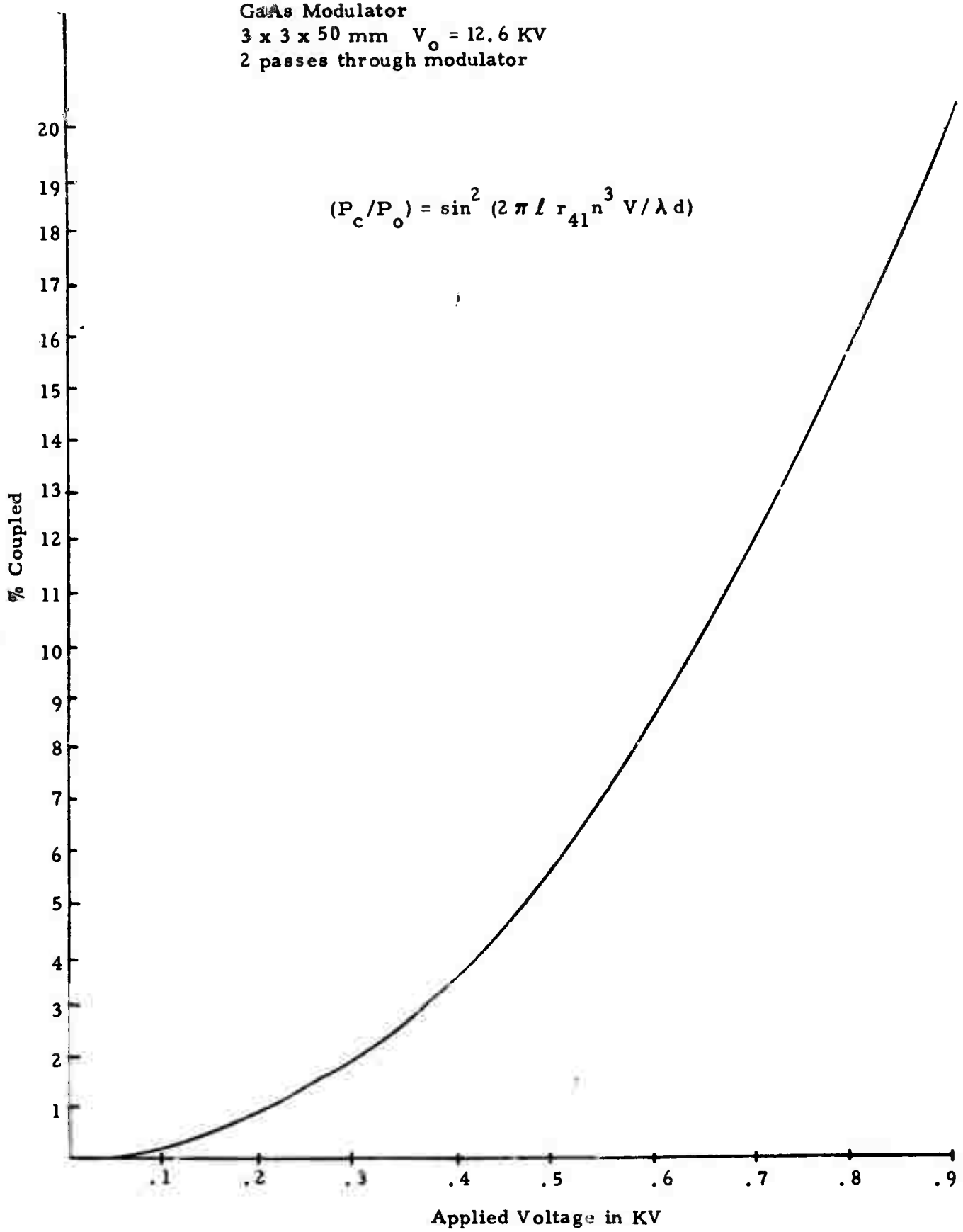

Figure 3.8. Theoretical Coupling Factor

The effect of increasing coupling is shown in Figure 3.9, which displays sampl of the intracavity pulse trains as observed through the 2% transmitting end mirror (M_6). In each trace the arrow indicates the pulse which was partially coupled. The actual coupling factors are slightly higher than the values determined from these traces, since the pulse completes a round trip through the gain medium before being observed at M_6. However, since the intracavity intensity is well above the saturation value, the corrections should be small.

The stability of the mode-locking is unaffected by the coupling. This is true even when the coupling is increased to the point of nearly extinguishing laser oscillation. This is illustrated in Figure 3.10, where the upper trace is the mode-locked pulse train observed at M_6, while the lower trace is the coupled output. The coupling voltage was applied during the period from the beginning of the trace to the second division mark from the left. During this period the laser pulse train is being quenched. After the voltage is removed the laser recovers with a time constant of approximately 5 μsec.

With coupling factors of less than 5%, recovery is practically complete within a single resonator round trip transit time. This makes it possible to consider using this technique to digitally code the laser output. Figure 3.11 shows the output pulse trains obtained by varying the duration of the coupling pulse. The coupling factor was approximately 5%. The pulse height envelope in the lower trace is due to the shape of the coupling pulse and does not reflect any recovery time effects. (The apparent difference in pulse height and width between the upper and lower figures is due to scale changes.)

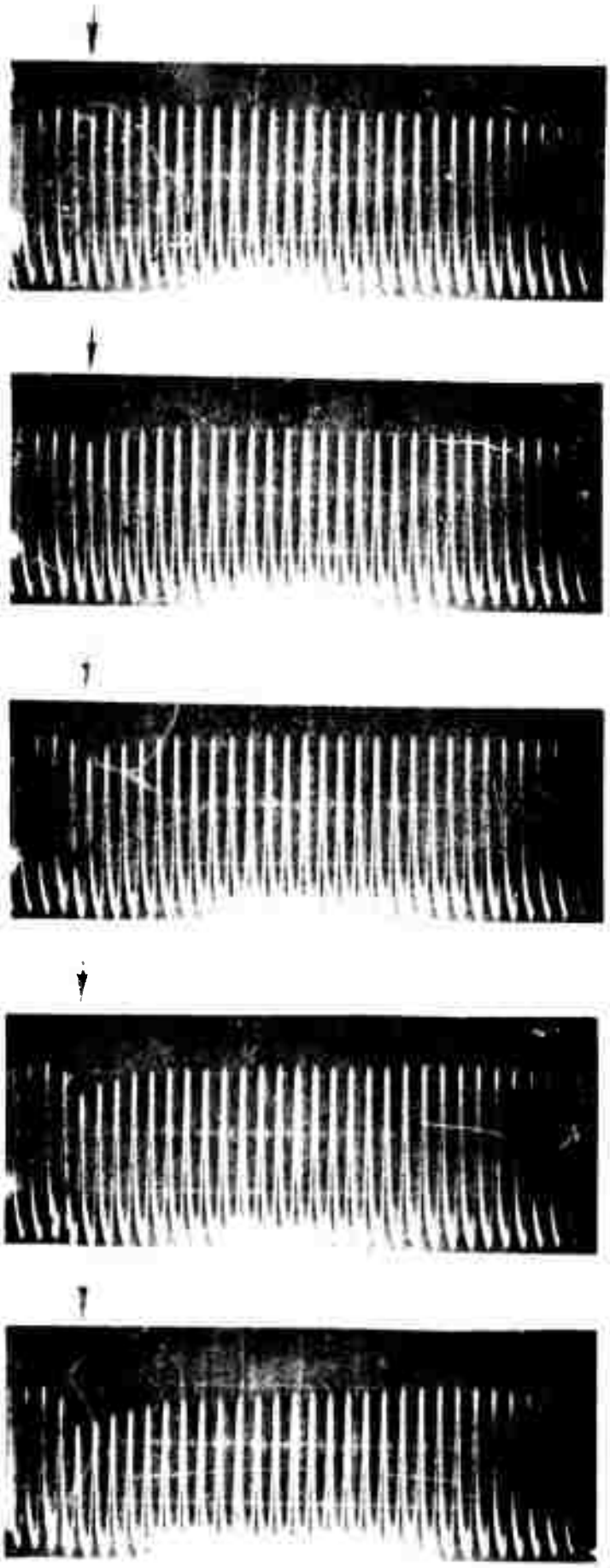

Figure 3.9. Effect of Coupling Factor Variation

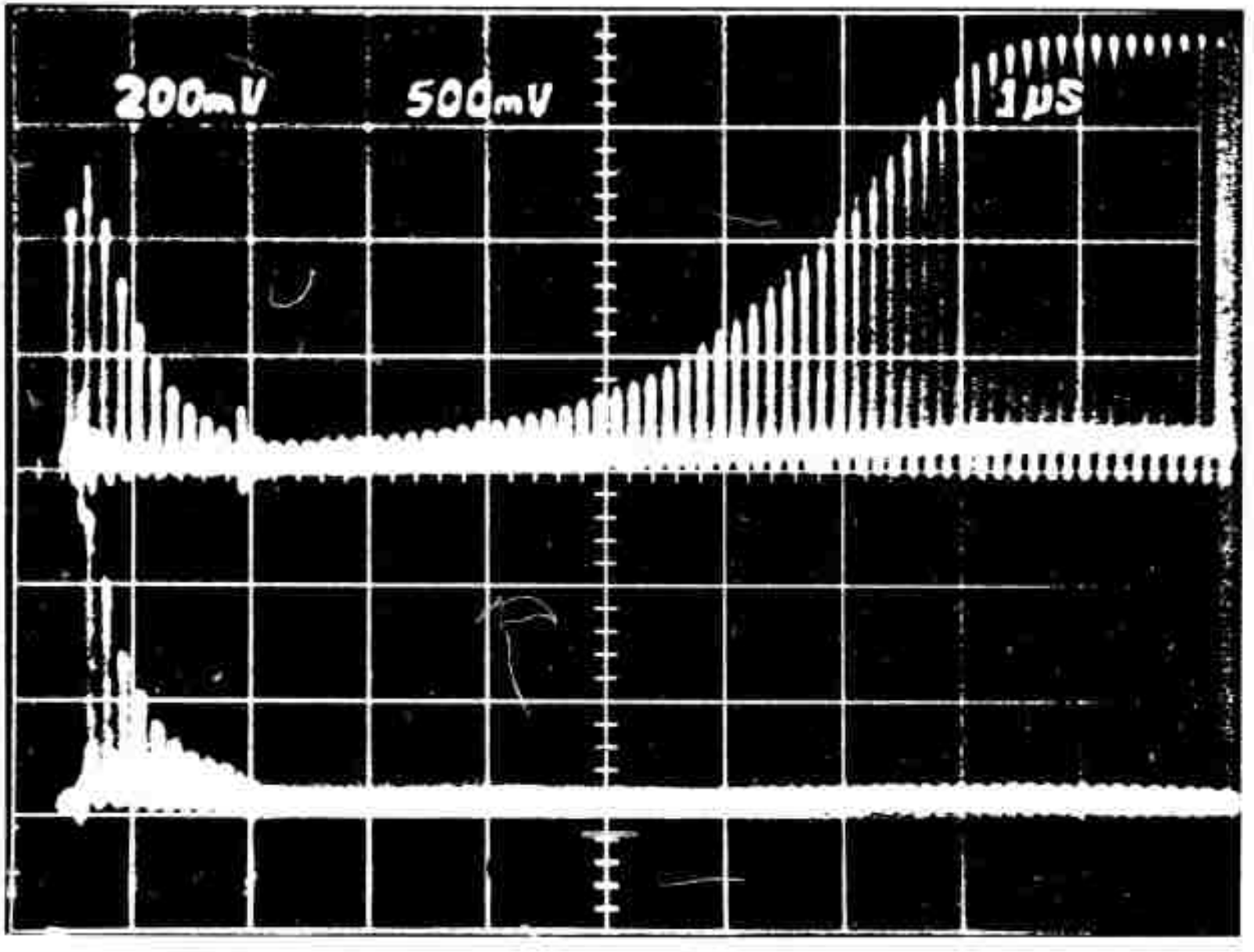

Figure 3.10. Laser output under over-coupled conditions.
Horizontal scale - 1 μs/div.
Dumping pulse of 2 μs/duration.

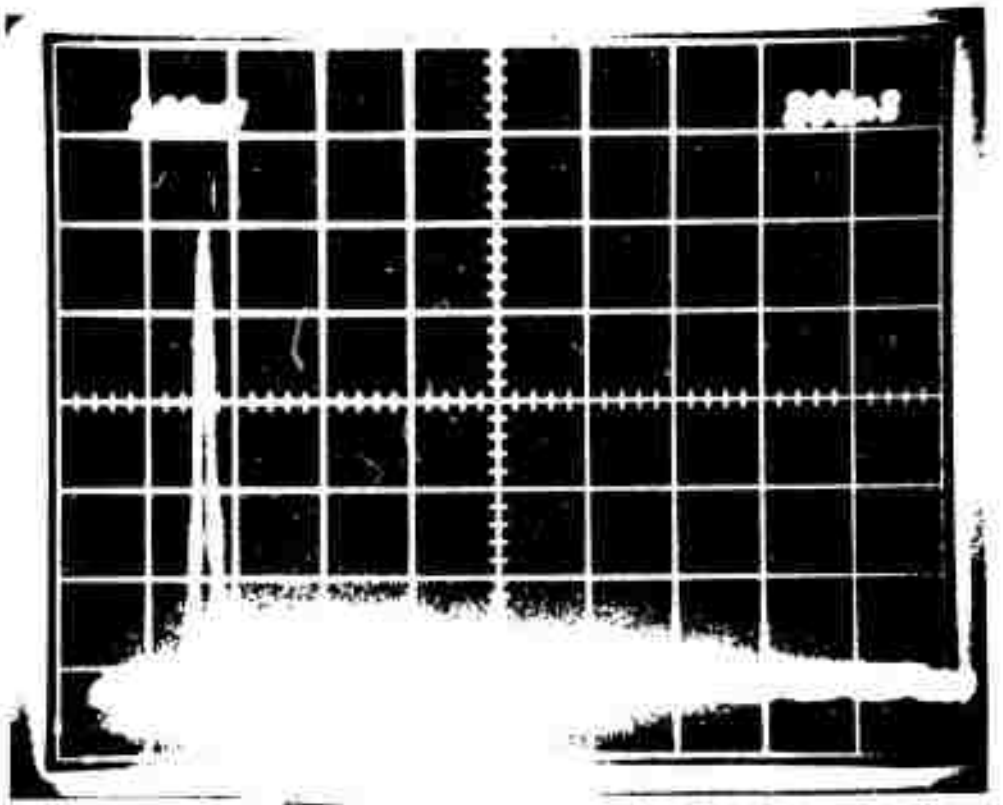

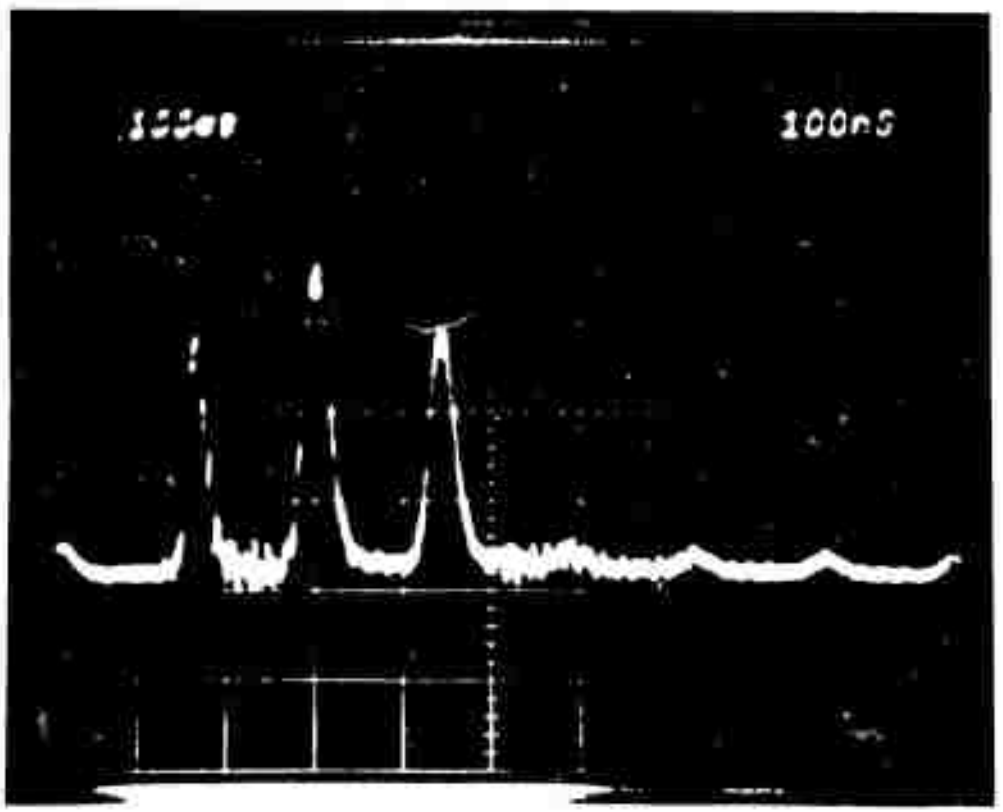

Figure 3.11. Coupled Pulses.
Upper Trace: Horizontal scale - 100 nsec/div.,
100 nsec dumping pulse.
Lower Trace: Horizontal scale - 200 nsec/div.,
400 nsec dumping pulse.

4.0 MODE-LOCKING THE CO_2 TEA LASER

Compared to the low pressure longitudinal discharge laser, the higher pressures accessible to the TEA laser offer the possibility of obtaining much narrower mode-locked pulses due to the pressure broadened line width. Experiments were performed with various TEA laser discharge configurations with the aim of exploiting this possibility. Loss-locking of the laser was accomplished by using the internal electrooptic element as an AM modulator. Attempts at phase-locking, however, were unsuccessful; and in an effort to understand this failure, a detailed investigation of TEA laser configurations and discharge was undertaken. This investigation included observations of the discharge medium by the use of a He-Ne probe beam and an image converter camera.

4.1 Linewidth of CO_2 TEA Lasers. The pulse width which may be attained by mode-locking a conventional, low pressure CO_2 laser is limited by the width of the gain line ($\sim$50 MHz) to approximately 20ns. A modest reduction in pulse width can be obtained at the expense of greatly increased modulator drive power by driving the modulator at a sufficiently high level to lock modes which are below the free running oscillation threshold. Appreciable reductions in pulse width and period can only be realized by employing a gain medium with increased bandwidth.

In conventional lasers, operating at pressures of less than 20 torr, Doppler broadening is the dominant mechanism determining the linewidth. At higher pressures, collisional broadening provides the dominant contribution to the linewidth. For a mixture of CO_2 and other gases, the collision frequency that determines the broadening of the CO_2 laser lines is given by

$$f_c = \sum_X \sigma\,(CO_2,\ X)\, n_X \langle v_{rel}\,(CO_2, X)\rangle_T, \qquad (4.1)$$

where

$$\langle v_{rel}\,(CO_2, X)\rangle_T = \sqrt{(8RT/\pi)(M_{CO_2}^{-1} + M_X^{-1})}$$

is the relative thermal velocity at temperature T, R is the gas constant, M's are molecular weights, n_X is the number of X molecule/cm^3, and

$$\sigma(X, Y) = \pi(d_X + d_Y)^2/4$$

is the "hard sphere" collision cross-section for a pair of molecules X and Y. The cross-section σ determined from kinetic experiments is usually a good approximation for the effective line broadening cross-section, since almost every collision interrupts the phase of a radiating molecule. The "hard sphere" diameters, d_X, are tabulated in the table below for several molecules of interest[12].

X	M	$d_X(\mathring{A})$
CO_2	44	4.00
CO	28	3.59
N_2	28	3.68
Ar	40	3.42
He	4	2.58

For typical laser gas mixtures at a total pressure of one atmosphere and a temperature of 300°K, the collision frequency f_c is approximately ~7GHz and the corresponding full linewidth at half maximum is given by $\Gamma = f_c/\pi \sim$ 2 GHz. Therefore pulse durations of < 1 ns and pulse repetition frequencies of > 200 MHz should be attainable.

Mode-locking of atmospheric pressure (TEA type) CO_2 lasers has been demonstrated by several investigators [13-15]. In these experiments, mode-locking resulted from nonlinear interaction in the gain medium (self-locking) or in a saturable absorber, and the resulting pulse durations were 2 - 8 ns. 1 ns pulses have been obtained by active locking using an acousto-optical loss modulator [16].

4.2 Experimental Configuration and Initial Experiments. TEA laser mode-locking experiments were attempted using the electrooptic techniques previously described. The initial experiments used pin cathode-bar anode discharges with the ballast provided by either a copper chloride electrolyte or by an array of carbon resistors. In these experiments a Tobe Deutschman ESB 122 pulse power supply (which was extensively modified for reliability, RFI suppression, and safety) was employed as the discharge source.

A 1 x 1 x 5 cm GaAs crystal was used for the TEA laser experiment to reduce the power density and minimize damage to the coatings. A 5M folded resonator configuration, diagrammed in Figure 4.1, was employed to obtain an axial mode frequency of 30 MHz which permitted the use of an available modulator driver.

The electrolyte ballasted discharge consisted of a 2M Brewster ended discharge tube which is shown in cross section in Figure 4.2. The pin electrodes are arranged with 2.0 cm separation. The active discharge area was approximately 1.0 cm by 2.0 cm with alternate rows in staggered positions. Cross flow between two plenum chambers was provided to insure uniform gas exchange along the length of the discharge. Initially, axial gas flow was employed, but the axial discharge repetition rate (1 - 10 pps) greatly exceeded the gas exchange rate. The GaAs crystal

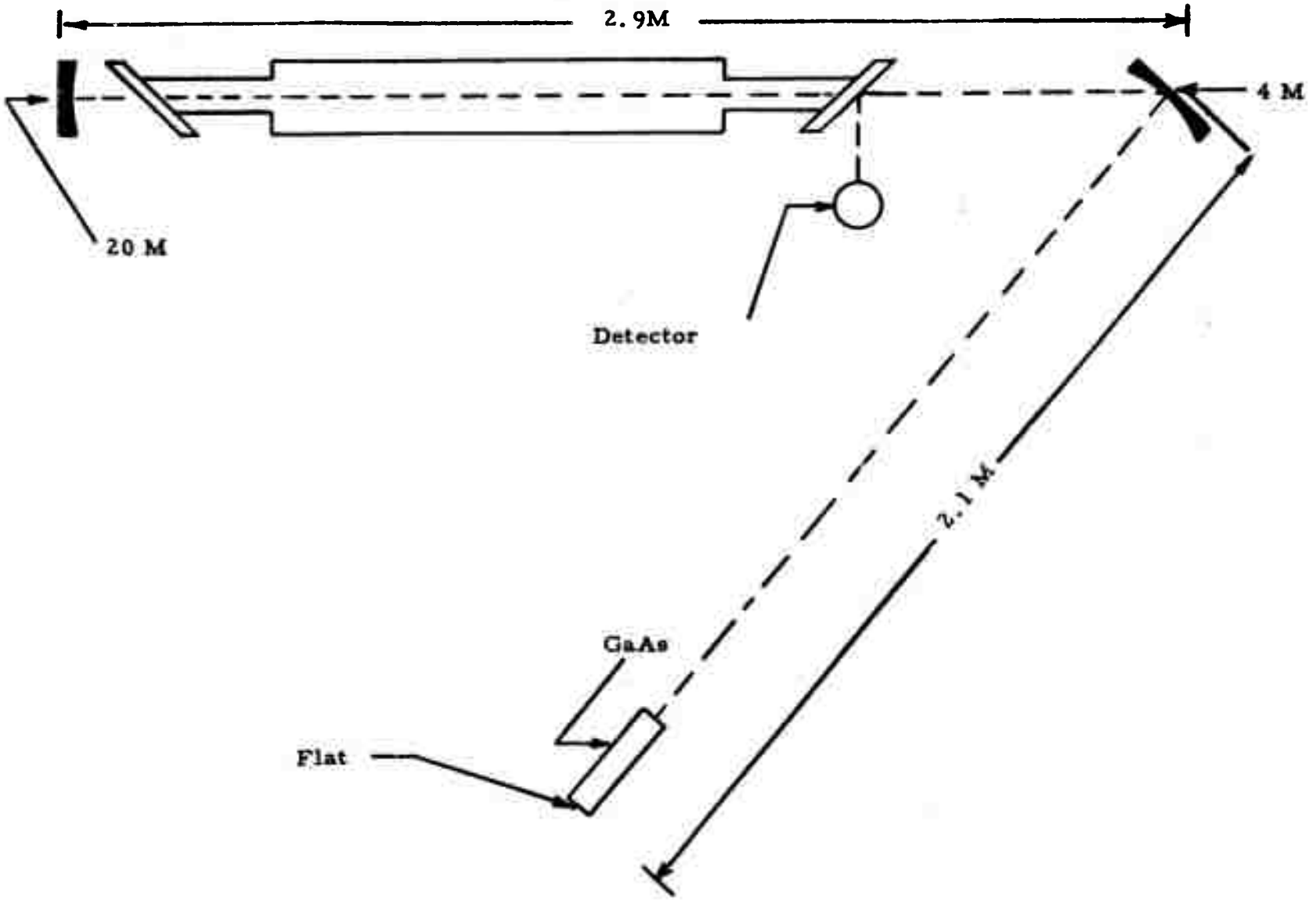

Figure 4.1. TEA Laser Mode-Locking Configuration

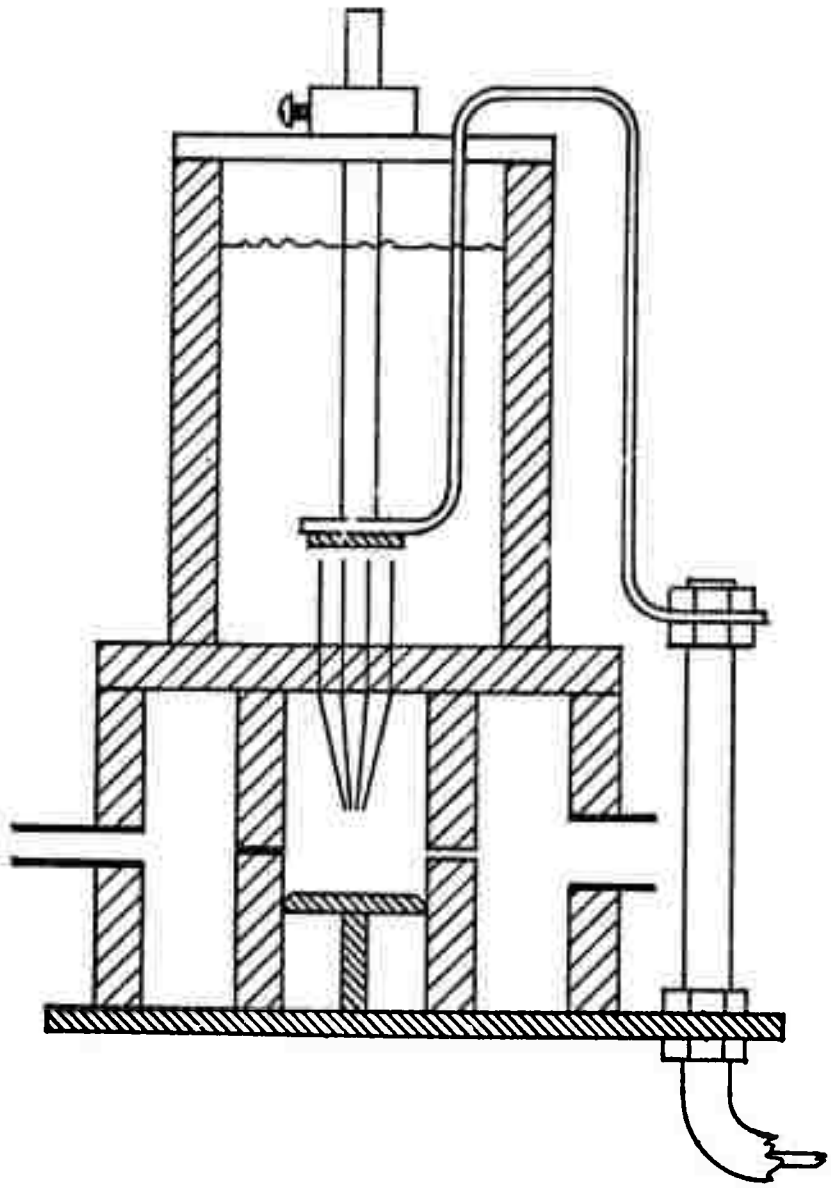

Figure 4.2. TEA Laser Discharge Electrode Configuration

used in experiments with this discharge had one of its $(1\bar{0}0)$ faces anti-reflection coated and the other gold coated to provide a total reflector.

The alternative resistor ballasted discharge consisted of a 1M long, pin cathode array of 100 carbon resistors (1K, 2 watt) separated by 2 cm from a solid copper anode.

Results, typical of either configuration but taken with the resistor ballast, are illustrated in Figure 4.3 where the output from a photon drag detector is displayed as a function of time. In this case, both of the $1\bar{1}0$ faces of the crystal were antireflection coated and a 5% coupling mirror was used to terminate the optical cavity. Electrical interference generated by the laser discharge is present during the first 2 μsec of Figure 4.3a (the oscilloscope was triggered on the discharge current rise); the actual laser output begins 3.5 μsec later with a 1 μsec wide envelope. The output here is multimode. Displayed on an expanded temporal scale in Figure 4.3b, the laser output is observed to be composed of a series of sharp spikes separated by the cavity round trip time (in this case 30 nsec) and illustrates the self-locking phenomenon.[14] Self-locking was observed in every shot with the depth of modulation and width of the spikes variable from shot to shot. Moving the laser medium to various positions within the optical cavity had no significant effect on the tendency to self-lock. With a 1 cm x 1 cm x 5 cm GaAs modulator interposed in the optical cavity, the increase in cavity losses, due to the irising effect and the increased insertion loss, was observed in the laser output. This increase in loss results in a longer delay between the exciting voltage pulse and laser output (typically 8 - 10 μsec).

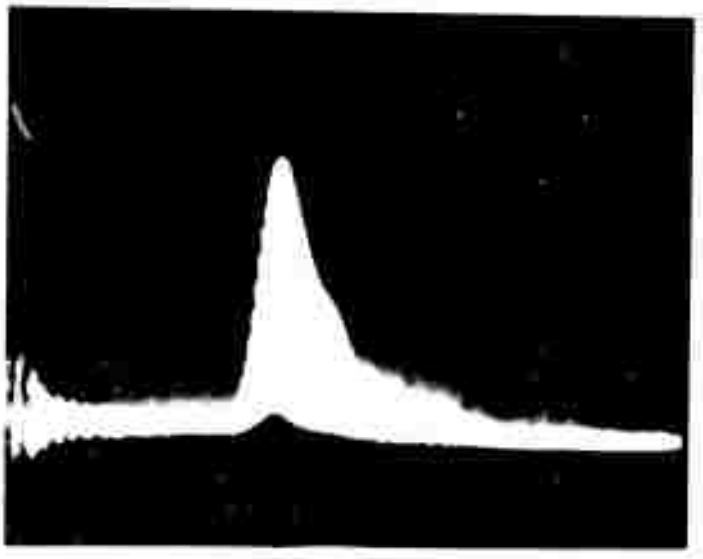

(a) 1 μsec

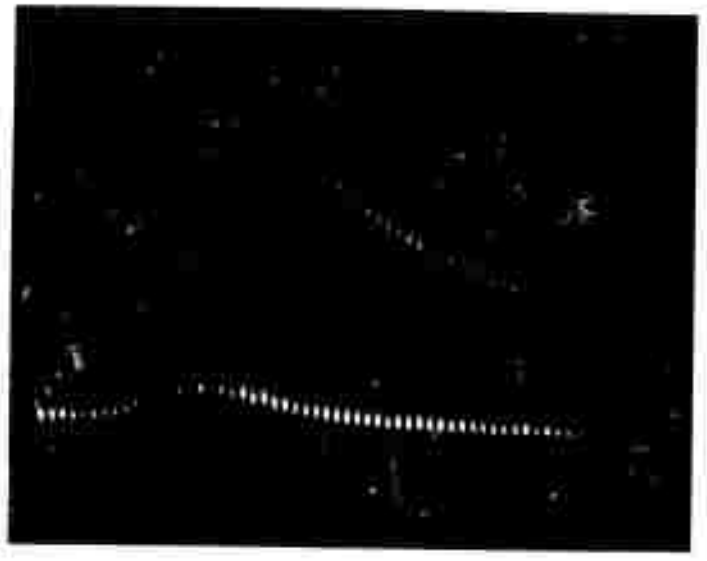

(b) 0.2 μsec

Figure 4.3. Self mode-locked pulse trains.

In the initial experiments, with either of the ballasting arrangements discussed above, the GaAs element was employed as a phase modulator as in the previous low pressure laser experiments. It was not possible to obtain reproducible locking which could be attributed to the modulator. The observed pulses were attributed to self-locking because the pulse shape was nearly sinusoidal indicating that only 2 or 3 modes were locked, and the depth of modulation varied considerably between laser pulses. It is believed that this behavior is attributable to the transient nature of the laser medium dispersion characteristics in the pulsed TEA laser which makes phase-locking difficult. This is discussed in Section 5.0.

4.3 Measurements of the Optical Quality of the Laser Medium. The failure of the initial phase-locking experiments and the instability of the laser output indicated that some measurements on the TEA discharge medium were in order. It was felt that the poor quality of the discharge could be responsible for the difficulties.

The common cathode pin discharge[17] leads to intense arcs which cause localized index of refraction changes. In this connection, two effects were considered: (1) the temporal development of the arc channel in the electrode gap, (2) the influence of neutral material and plasma ablated from cathode surfaces[18] at the sites of visibly intense cathode spots.

An image converter camera (I.C.C.) was used to obtain framing photographs of a pin discharge and results are shown in Figure 4.4. Each of the numbered frames is a 20 ns exposure of a 12 pin section of the discharge, with the pin cathodes at the top and the bar anode at the bottom. Frame 1 was triggered on the initiation of the discharge current, frame 2 was exposed 200 ns later, and frame 3 was exposed 200 ns after

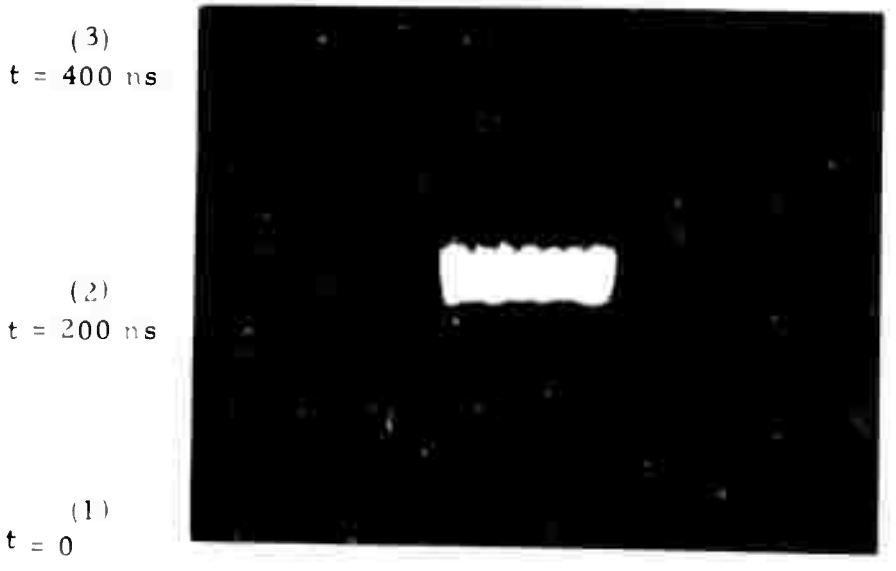

Figure 4.4 Image converter camera framing photographs of TEA laser pin discharge.

frame 2. The original of the photograph showed a faint pin discharge in frame 3 which is difficult to see in the reproduction. The data indicates that the arcs are fully developed within 200 nsec of the start of the current pulse and remain luminous for about the width of the current pulse (500 nsec). If it is assumed that the gas heated by the arcs propagates at acoustic velocities, then over the 5 - 10 μsec period between the creation of the arcs and the time of laser output, the heated gas will not have travelled very far and could not have caused local index variations to the laser radiation.

The deviation of a He-Ne beam was used as a diagnostic probe of the relative index changes in the medium (the experimental set up is illustrated in Figure 4.5). With the discharge off, the beam was first aligned with the center of the laser tube followed by an iris and a GeAu detector. It was found that the pulsed discharge caused the beam to deviate only in the upward direction, toward the cathode pins, with a deflection of approximately 2 mm over a 4M path. Lateral displacement was not observed, since index changes due to the heated gas in the arc channel were apparently weak compared to the index changes causing the upward deflection.

The detector output is shown in Figure 4.6 for a fill pressure of 200 torr. In the quiescent state, that is without a discharge and hence without beam deviation, the He-Ne beam is aligned with the iris and the detector reads maximum intensity. This is defined as the dc level and is positioned in the center of the oscilloscope traces. Decreasing He-Ne beam intensity is in the negative direction from the dc level and this corresponds to increasing beam deflection. Figure 4.6a indicates that the beam experiences maximum deflection at approximately 1 msec after the discharge and relaxes

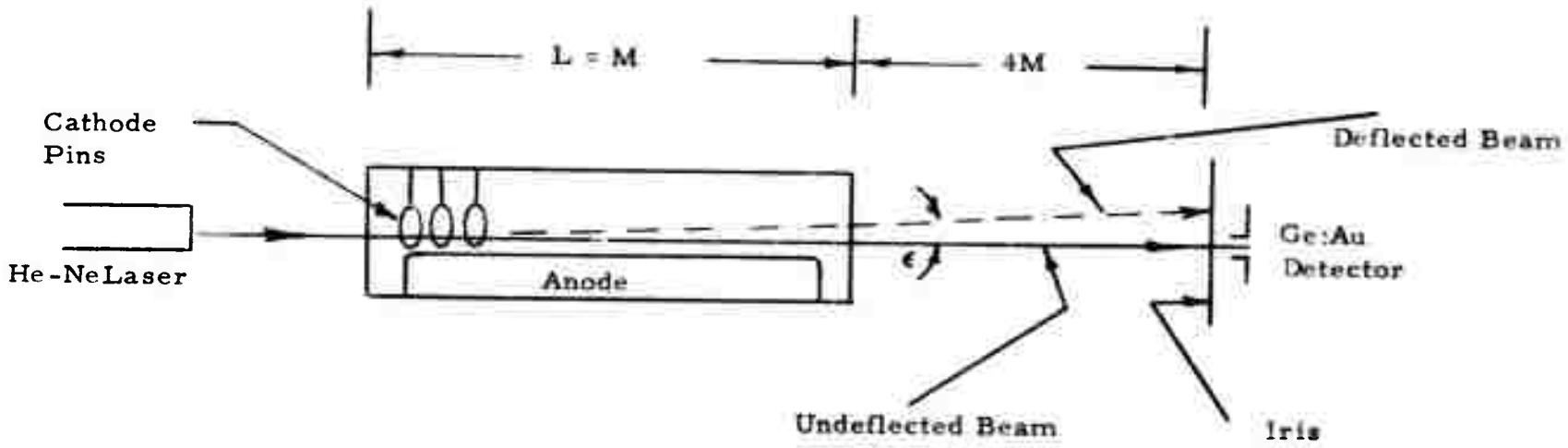

Figure 4.5. He-Ne laser probe configuration.

to the dc level in approximately 15 msec. In figure 4.6b the time scale has been expanded, and the vertical gain increases by 4. The deflection is observed to be 20% of the maximum, 10 μsec after the discharge. The closer the probe beam is aligned to the cathode pins, the sooner the deflection occurs. In addition, as the fill pressure is increased, the time to reach the maximum beam deflection increases as shown in Figure 4.7, (same vertical gain as Figure 4.6a) for a pressure of 500 torr. At these higher pressures, the discharge becomes erratic with many of the pins failing to ignite.

These observations suggest that the cathode pins are the sources of a highly refractive material which streams into the electrode gap. Such material is quite possibly composed of vapor and plasma produced during the formation of cathode spots. The contribution of neutral gas and plasma to the index η, can be formulated as follows:[19]

$$\eta = 1 - 1/2 \frac{\nu_p^2}{\nu^2} + 2\pi \sum_a \alpha_a n_a ,$$

where $\nu_p^2 \cong 10^8 n_e \text{ sec}^{-2}$ is the electron plasma frequency,

n_e is the electron density expressed in cm^{-3},

$\nu = 3 \times 10^{15} \text{ sec}^{-1}$ is the He-Ne laser frequency, assumed large compared to the electron-neutral collision frequency,

α_a is the polarizability of atomic species a, and

n_a is the density of atomic species a.

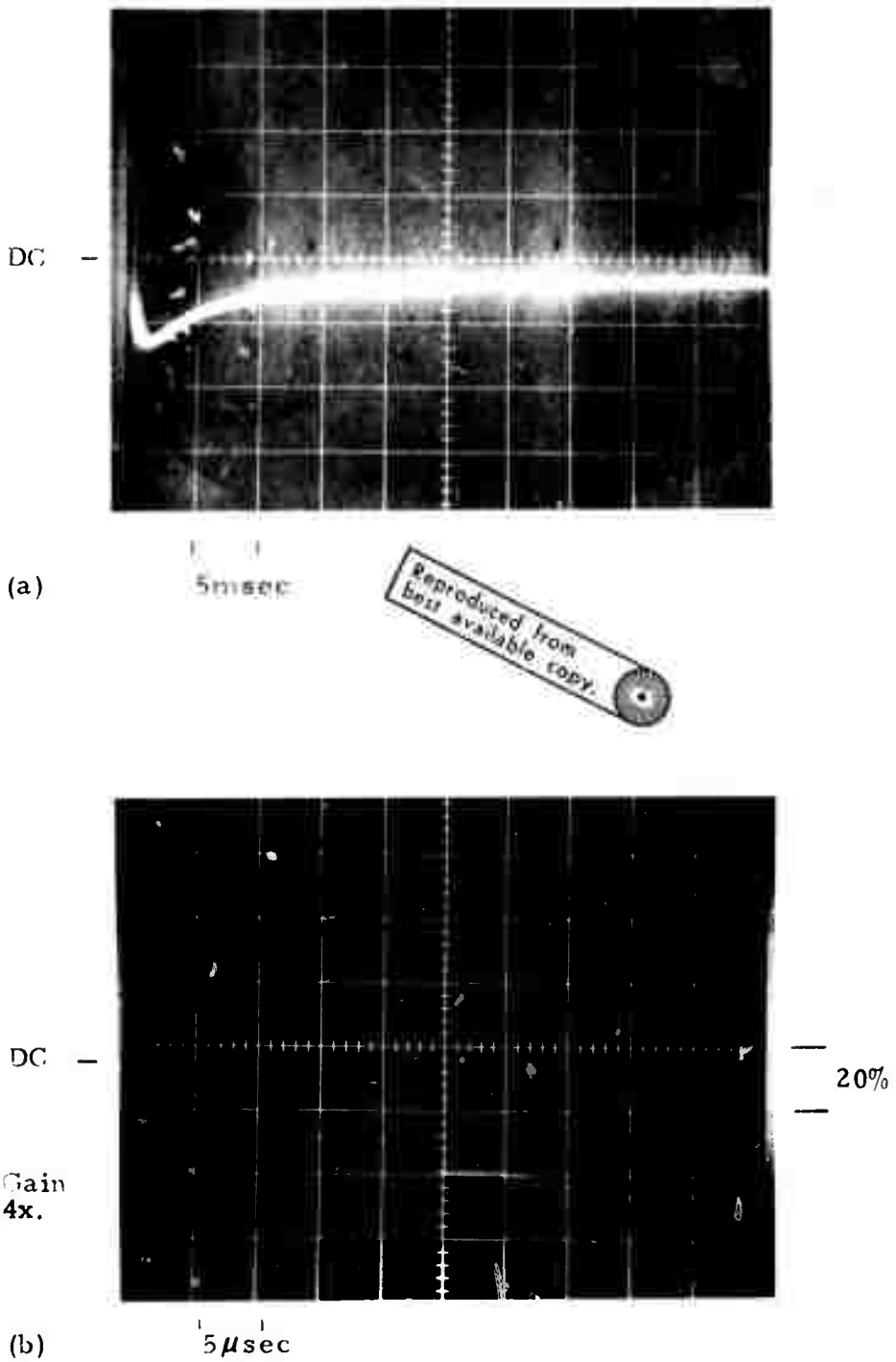

Figure 4.6. He-Ne laser probe detector output at low pressure.

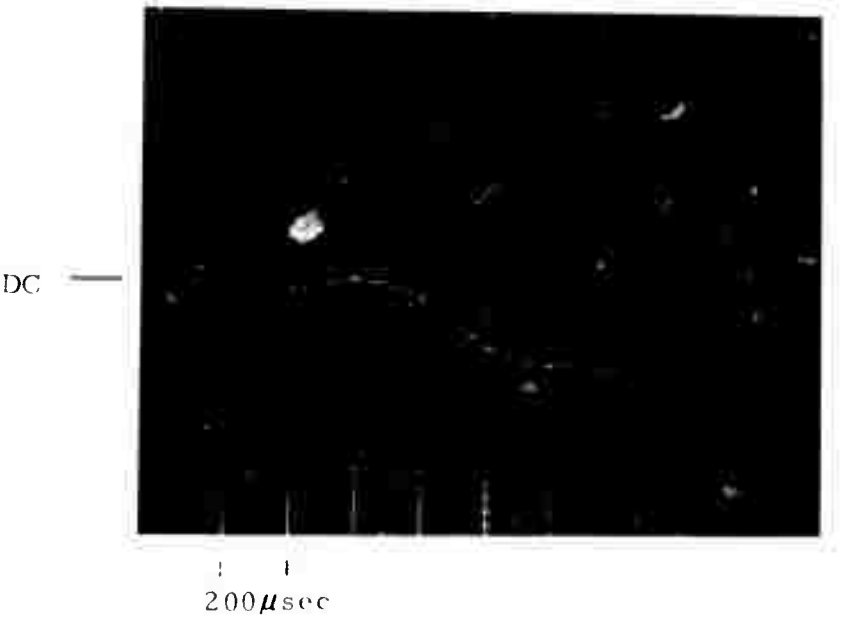

Figure 4.7. He-Ne laser probe detector output at high pressure.

The angular deflection ϵ, defined in Figure 4.5, is related to variations in the index according to

$$\epsilon = L/n \ dn/dy$$

where ϵ is in the direction of the coordinate y.[20] This shows that the effects of the plasma and neutral densities are opposing: the plasma tends to force the beam down and the neutrals force it up. The neutral contribution was clearly dominant in the experiment.

The various processes discussed above are summarized in Figure 4.8, where their relative temporal behavior is plotted schematically.

4.4 Modifications of the Discharge Configuration to Improve Medium Optical Quality. In an attempt to improve medium homogeneity, a 3 electrode[21] and helical resistor pin discharge configurations were developed. The 3 electrode scheme, shown in Figure 4.9, consists of a solid anode and stainless steel mesh cathode 1.5m long, stretched tightly around, but insulated from, a bar trigger electrode which is returned to ground through (12) 920 pf capacitors distributed along its length. Voltage from a 0.05 f capacitor, charged to 20 kV, is switched to the mesh cathode whereupon a weak discharge (limited by the trigger capacitor) is initiated to the adjacent trigger electrode preliminary to the main discharge. The result is a uniform preionization of the medium surrounding the cathode surface, and correspondingly uniform discharge in the main gap.

For pressures below about 300T, with a mixture of 83.5% He, 12% N_2, 4.5% CO_2, the discharge is observed to ignite in a uniform glow with the exception of about 10 - 20 weak filamentary arcs occurring at random positions. Above 300T, several bright arcs are formed. The main gap

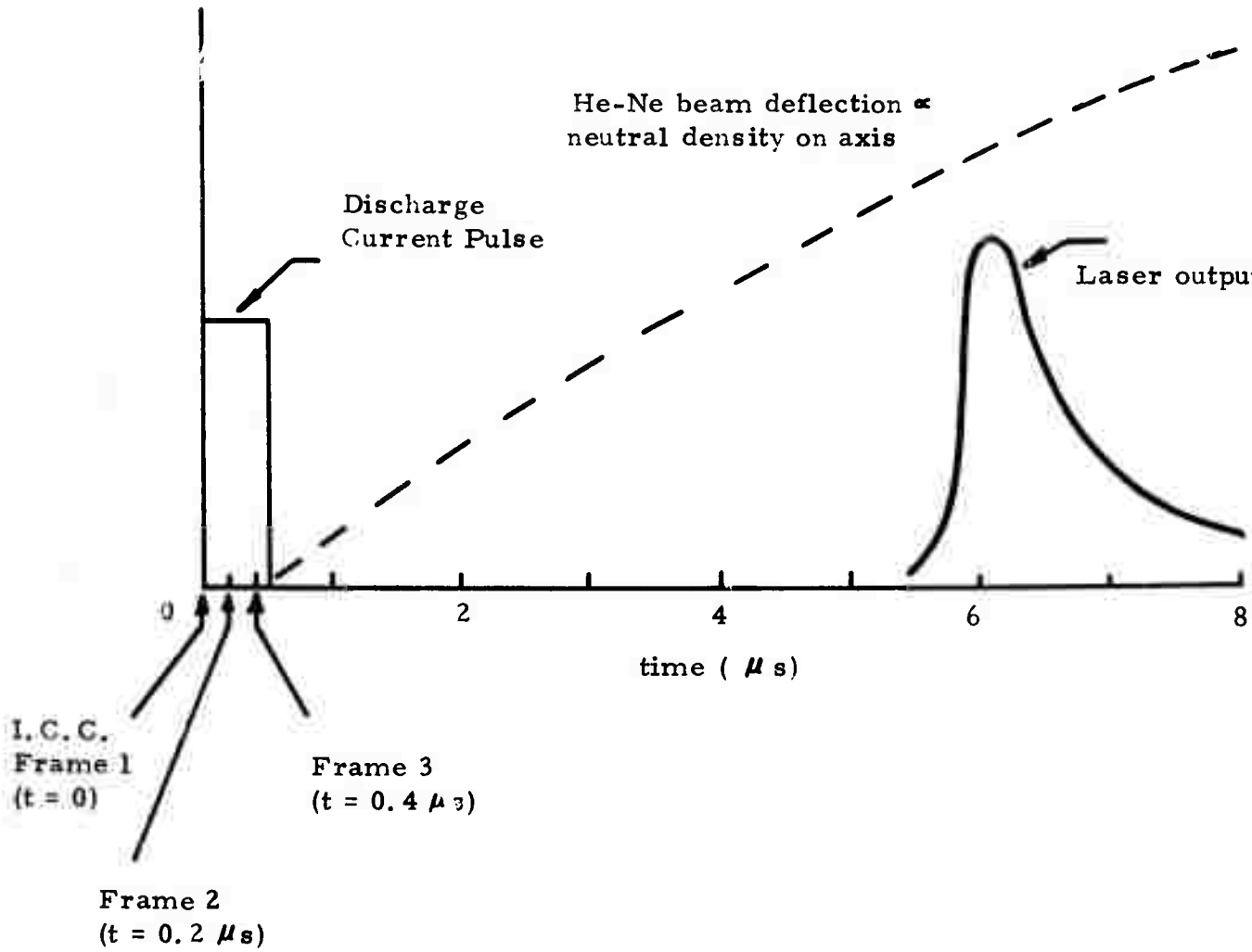

Figure 4.8. Schematic representation of important TEA laser processes.

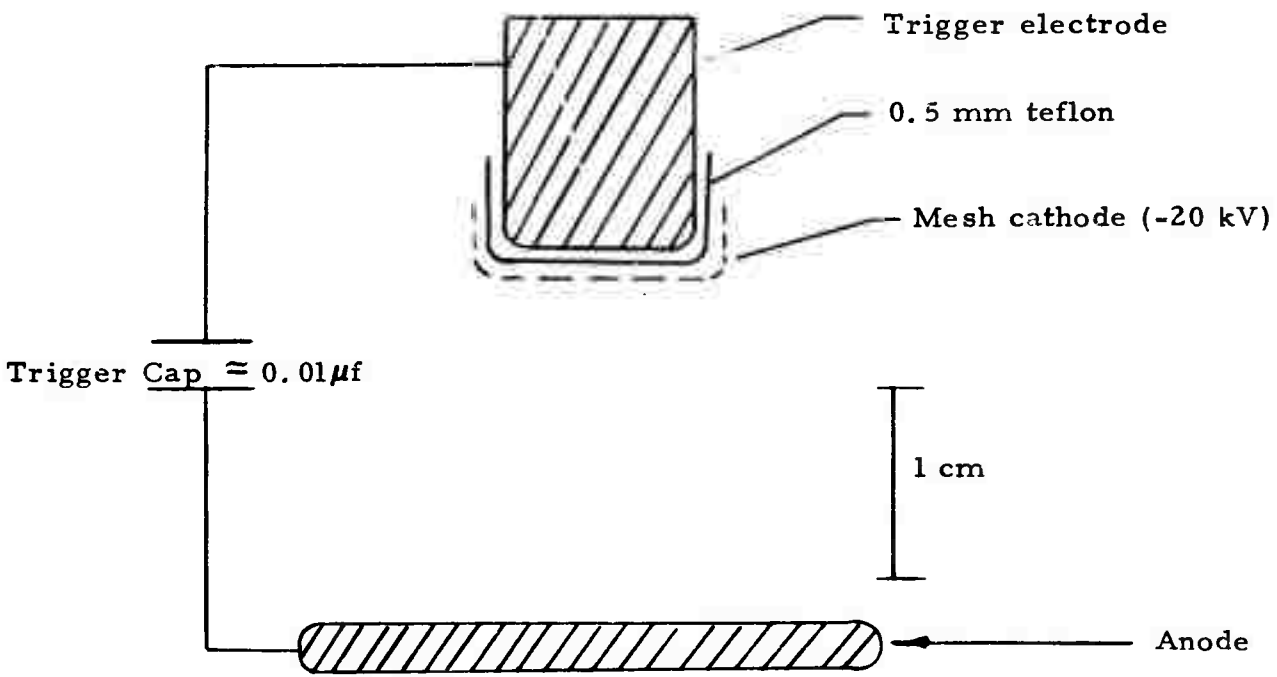

Figure 4.9. TEA laser three electrode configuration.

spacing, mesh density, and trigger capacitor were adjusted so as to minimize arcing. Cathode spots were also observed over the entire mesh area which, although not nearly as intense as those accompanying pin discharges, nonetheless had the same effect of significantly deviating a He-Ne probe beam toward the cathode.

It was thought that since beam deflection resulting from cathode spots could not be eliminated even in the highly uniform 3 electrode arrangement, the action of the cathode spots could at least be averaged out with a helical discharge geometry. This led to the construction of a helical, resistor pin, TEA laser configuration described below.

Stainless steel screws were threaded into a series of holes describing two opposing helices of two revolutions on a 1 m long, 4 cm ID plastic tube. (Steel screws were chosen over the usual copper resistor pin electrode in order to minimize the ablation of metal.) Carbon resistors (1k, 2 watt) were soldered to the screws of one helix; and the screws of the other helix, acting as pin anodes, were connected in parallel and separated by 2.5 cm from the cathode array.

The He-Ne beam, when aligned with the center of the tube, was found to expand uniformly about its center during the discharge with no deviation in any preferred direction. When aligned off axis, the beam was seen to deflect toward the pins on the near side, since material ablated from these pins reached the beam before that ablated from the opposing pins.

4.5 Phase-Locking with Modified Discharges. Phase-locking experiments were carried out with each of the discharge configurations, discussed above, in the experimental configuration shown schematically in Figure 4.10. In

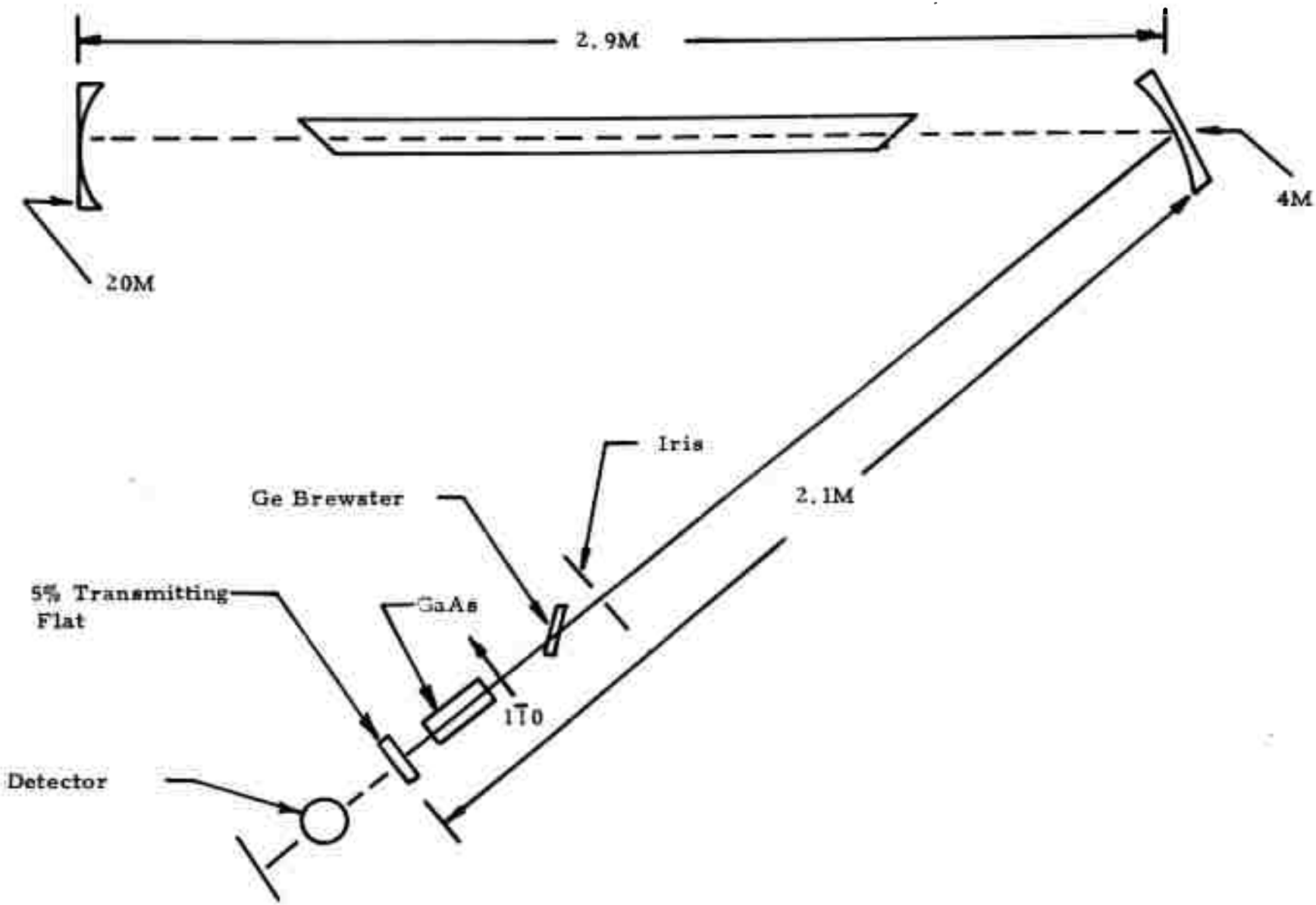

Figure 4.10. TEA laser mode-locking configuration.

all cases, approximately -20 kV from a 0.05 μf capacitor was switched to the cathode assembly. Laser output was monitored directly with a photon drag detector. The combined rise time of detector, amplifier, and oscilloscope was approximately 4 nsec. The laser gas mixture (4.5% CO_2, 12% N_2, 84.5% He) was held below 300T, since above this pressure the formation of intense streamers degraded the laser output. An rf transmitter and linear amplifier output, tuned to the axial mode difference frequency and impedance matched with a matching network was applied across the GaAs crystal faces with a maximum peak to peak voltage of 3 kV. As discussed previously, the laser output pulse was consistently self mode-locked with essentially a sinusoidal modulation, indicating the participation of only 2 or 3 axial modes. This modulation was easily distinguishable from that which would result from successful externally imposed mode-locking, since the latter would affect the locking of many more axial modes. It was found, however, that consistent and reproducible pulse trains indicating phase-locking could not be obtained, most probably due to the transient nature of the gain medium.

Attempts at loss-locking, however, were successful. In this case, 2 kV peak-to-peak at the axial mode frequency was applied to the 110 crystal faces. The cavity optical field vector was polarized by the Brewster plates along 110 direction. The voltage applied to the modulator coupled some of the cavity power into the cross polarization which was reflected off the Brewster plates and lost. The loss was time varying at the modulation frequency and occurred by exactly the same mechanism as in the pulse dumping technique described previously. Typical results are shown in Figure 4.11, where the pulse train shows significant departure from a simple sinusoid. The narrower pulses indicate that loss-locking locks significantly more modes than the self-locking. Pulse widths of 10 nsec were typical with some variation from shot to shot.

50 ns

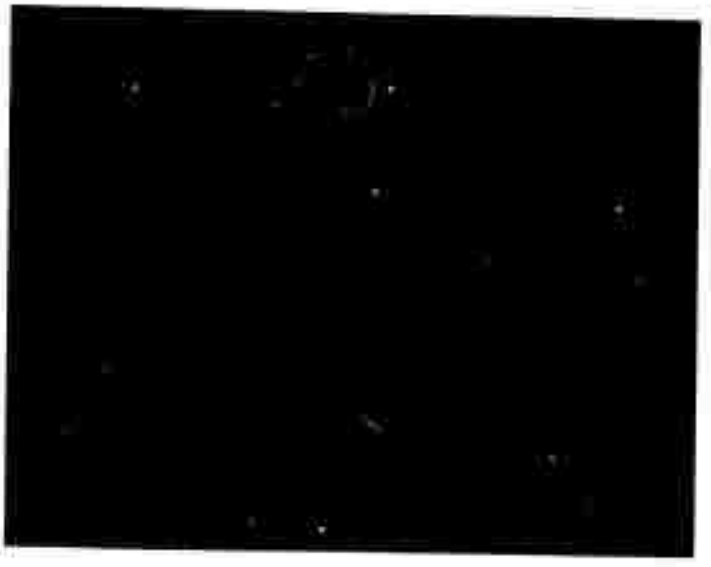

20 ns

Figure 4.11. Loss Mode-Locked Pulse Trains.

The results of the experiments with TEA lasers, discussed above, indicate that the transient nature of the gain medium limits the applicability of phase modulation to mode-locking of TEA lasers. A discussion of various mode-locking phenomena, in the special case of a transient gain medium, is presented in the next section.

5.0 DISCUSSION OF MODE-LOCKING PHENOMENA

It is apparent from the experimental results that the modes of a TEA laser have a strong tendency to self-lock and can be loss-locked but cannot be phase-locked. In this section, it is shown how the observed behavior may be explained in terms of the processes involved in mode-locking. First we shall briefly discuss each of these mode-locking phenomena in order to understand the process.

5.1 Self Mode-Locking. The pulsing behavior of lasers was observed in the early experiments but was not explained until the concepts of self mode-locking were developed. Several authors[22, 23, 24] have investigated the effect and have offered explanations which qualitatively explain the results. Measurements have been made on the tendency to self-lock and on the repetition frequency of the pulses as a function of the position of the gain medium in the cavity, and the pumping level of the gain medium. Most of the measurements have been made using the He-Ne laser.

The locking can be explained by a third order nonlinearity of the gain medium.[25] The plasma medium possesses inversion symmetry and hence the lowest order nonlinear terms in the susceptibility are third order. This nonlinearity produces a polarization proportional to the cube of the electric field. Near a resonance, these nonlinear terms can become sufficiently intense to act as injection-locking signals on nearby modes, and cause frequency pulling and affect a fixed phase relation between all the longitudinal modes.

Consider three modes at ω_n, ω_{n-1}, and ω_{n+1}, where $\omega_{n+1} - \omega_n = \omega_n - \omega_{n-1} = \Delta\omega$ with phases ϕ_n, ϕ_{n-1}, and ϕ_{n+1}. The nonlinear process

$$P(\omega_{n+1}) = \chi^{(2\omega_n - \omega_{n-1})} E(\omega_n)\, E(\omega_n)\, E^*(\omega_{n-1})$$

produces a polarization at ω_{n+1} which acts as a locking signal to the ω_{n+1} mode. Likewise a polarization is generated at ω_{n-1} by the nonlinear mixing of $2\omega_n$ and ω_{n+1}.

The modes are no longer free running but pick up a phase given by the injected polarization. The mixing process requires that

$$\phi_{n+1} = 2\phi_n - \phi_{n-1}$$

and hence that there be a linear phase progression between the modes, or that $\phi_{n+1} - \phi_n = \phi_n - \phi_{n-1} = \Delta\phi$. The nonlinear susceptibility therefore gives a comb of modes uniformly spaced in frequency with an arbitrary phase step ($\Delta\phi$) between neighboring modes. This mode frequency spectrum is a train of pulses when transformed into the time variable.

5.2 Loss Mode-Locking. In this case an amplitude modulator is placed internal to the laser cavity and driven at one half the longitudinal mode spacing frequency. The mode-locking can be explained in the frequency domain in the same way as in the self-locked case by considering the side bands generated as injection locking signals to the other modes. For an electrooptic amplitude modulator, with no dc bias voltage applied, the first side bands occur at $\omega_c \pm 2\omega_M$ where ω_c is the carrier frequency and ω_M, the modulator drive frequency which must be equal to c/4L to couple neighboring modes to each other.

Kaminow[26] has shown that the output of an amplitude modulator in the same polarization as the input can be written as

$$E(t) = E_o \left\{ \left[1 - \left(\frac{\pi V}{4 V_{\lambda/2}} \right)^2 \right] \cos \omega_c t \right.$$

$$\left. - 1/2 \left(\frac{\pi V}{4 V_{\lambda/2}} \right)^2 \left[\cos (\omega_c + 2\omega_M) t + \cos (\omega_c - 2\omega_M) t \right] \right\}$$

The modulator is driven by $V \cos \omega_M t$ and has a half-wave voltage of $V_{\lambda/2}$. This expression shows that the modulator imposes a $\pm \pi$ phase shift. shift on the side bands relative to the carrier. If each mode is to act as a carrier frequency to inject side bands into its neighboring modes, the modes must lock with a linear phase progression of π between the modes. In the time domain this is a series of pulses which pass through the modulator at the time when $2\omega_M t = \pi$ or when the applied voltage passes through zero. This means that the pulse, oscillating back and forth in the cavity, passes through the modulator at the correct time to have a minimum round trip loss.

5.3 Phase Mode-Locking. In this case the internal modulator is a phase modulator driven at the longitudinal mode spacing frequency. However the locking cannot be explained on the basis of injection locking of neighboring modes. Consider the GaAs electrooptic modulator used as a phase modulator and assume the modulation signal is $V \sin \omega_M t$. The output of the modulator can be shown to be[27]

$$E(t) = E_o \left\{ J_o(m) \cos \omega_c t + J_1(m) \left[\cos (\omega_c + \omega_M) t \right. \right.$$

$$\left. - \cos (\omega_c - \omega_M) t \right] + J_2(m) \left[\cos (\omega_c + 2\omega_M) t \right.$$

$$\left. \left. + \cos (\omega_c - 2\omega_M) t \right] \text{-----} \right\}$$

where $m = \pi/2\ (V/V_{\lambda/2})$, where $V_{\lambda/2}$ is the half wave voltage of the modulator as used for the amplitude modulation case. We see that the upper first order side band is in phase with the carrier, but the lower first order side band is $\pm\pi$ out of phase. There is no set of phases that the modes can assume for each to act as the carrier to inject side bands into its neighbors. As discussed below, the phases of the modes of a phase-locked mode train actually assume a $\pi/2$ phase progression between the modes. This clearly cannot be explained by side band locking.

The mode-locking is a much more subtle process and has been explained by Siegman and Kuizenga[28] as an interaction and balance between the effects of the phase modulator and the gain medium. If the phase modulator shifts the phase of the optical wave by $\phi_m \sin \omega_M t$, the total phase of the optical wave as a function of time is

$$\phi(t) = \omega_c t + \phi_m \sin \omega_M t$$

and the frequency of the wave is

$$\omega(t) = d\phi(t)/dt = \omega_c + \omega_M \phi_m \cos \omega_M t.$$

If the pulse is short compared to the modulation frequency, then all of the frequencies of the pulse are shifted by $\omega_M \phi_M \cos \theta_M$, where θ_M is the phase of the pulse relative to the modulation frequency as shown in Figure 5.1. If the pulse passes through the modulator at any phase except $\theta_M = \pi/2$ or $3\pi/2$ it will receive a linear frequency shift. If this shift is not balanced out by an opposite shift due to the gain medium, the pulse is unstable since it will eventually be shifted out of the linewidth of the gain medium as it shuttles back and forth in the cavity.

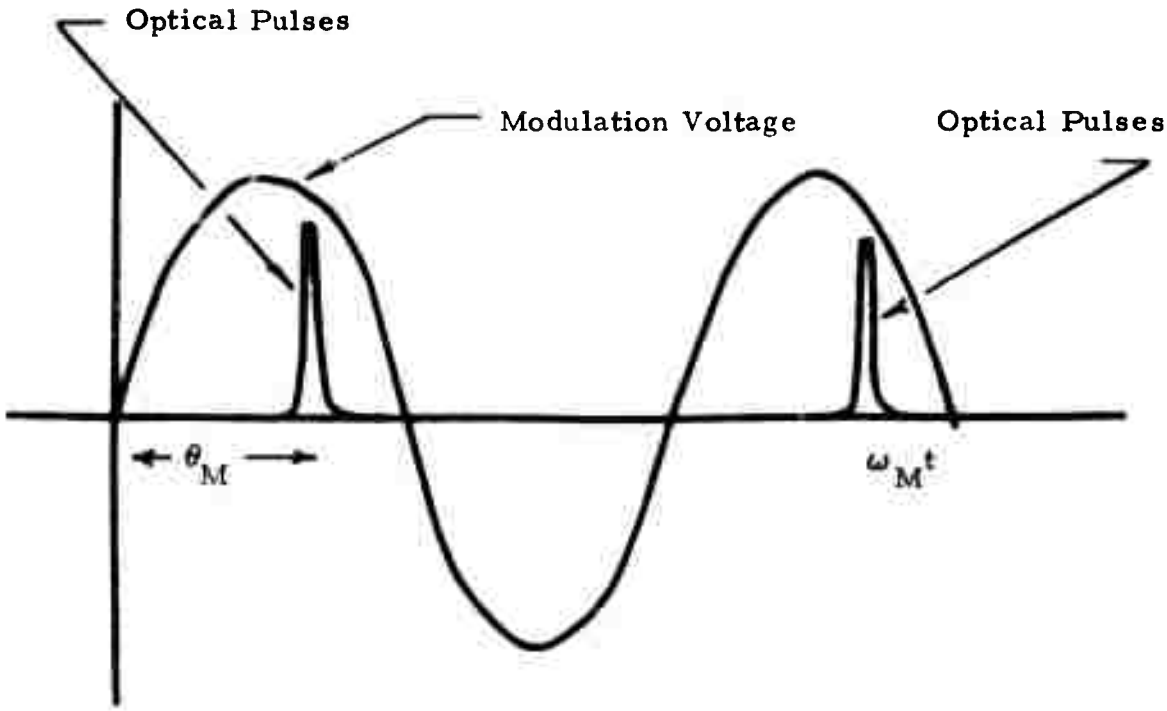

Figure 5.1. Relative laser pulse and modulator phase shift.

Siegman and Kuizenga[29] have shown that if ω_M is exactly c/2L a stable mode-locked train is possible as follows. The pulses pass through the modulator at $\theta_M = \pi/2$ or $3\pi/2$ and receive no frequency shift. In the frequency domain, the progressive phase shift between the longitudinal modes is then $\pi/2$ or $3\pi/2$. The pulse carrier frequency is centered on the laser line so the gain medium does not pull the pulse frequency. This solution is stable and the chirping on the pulse can be predicted from the effects of the modulator.

If the modulation frequency is slightly detuned from c/2L, the situation is more complex but can be explained as follows:

i) The pulse round-trip transit time must adjust itself to remain equal to $2\pi/\omega_M$. This can be done either by changing the pulse group velocity or by the chirp on the pulse as it passes through a dispersive medium. The magnitude of the velocity changes, due to either effect, is determined by how far the pulse carrier frequency is shifted from the laser line center.

ii) If the pulse carrier shifts off of line center to adjust the transit time, the pulse will receive a frequency shift when it passes through the medium. This shift is due to the higher gain at line center which causes the center of gravity of the pulse to be pulled toward line center.

iii) This frequency shift of the gain medium must be balanced by an opposing frequency shift in the modulator to maintain a stable situation. The pulse therefore passes through the modulator at a phase slightly off from $\pi/2$.

5.4 Qualitative Explanation of Experimental Results. From the above discussion it is clear that self mode-locking and loss-locking are similar phenomena. Both can be explained on the basis of injection locking by side bands. It is reasonable to expect then that a medium which tends to self-lock can be loss-locked. The loss modulator determines the timing of the pulses relative to the modulation voltage. The nonlinearity of the medium will enhance the locking established by the modulator since the side bands created by the medium nonlinearity can assume the same phase as those created by the modulator. It is also reasonable to expect these locking phenomena to be independent of moderate temporal fluctuations in the laser medium gain and dispersion since there is no balance to be maintained between the modulator effects and the effects of the gain medium. To first order, this mode-locking process is independent of the magnitude of the laser gain or the laser dispersion.

However quite the opposite is true for phase-locking. It takes several round trips for a mode to be established, i.e., its frequency and phase are not well defined until the interference effects of several round trips are established. In phase mode-locking the relative phases of the longitudinal modes are partially determined by the gain and dispersion of the laser unless ω_M is exactly c/2L. If the laser medium changes with time, the mode phases must change to maintain mode-locking. If the medium is fluctuating in time on the order of a few round trip times, the mode phases and frequencies cannot change rapidly enough to maintain a mode-locked train. The TEA laser pulse is approximately one microsecond long, which for our cavity is only 30 round trips. Hence it appears that the gain and dispersion may not be constant enough in time to ever establish a steady state phase-locked mode train.

In the experiments on phase-locking of a longitudinal discharge laser, the gain medium was operated cw and a shutter placed in the cavity to control the duty cycle. The success of phase mode-locking in this case can be attributed to the temporal stability of the gain medium characteristics during the lasing pulse.

6.0 REFERENCES

1. M. M. Mann, R. G. Eguchi, W. B. Lacina, M. L. Bhaumik and W. H. Steier, Appl. Phys. Letters 17, 393 (1970).

2. R. G. Eguchi, W. H. Steier, M. M. Mann, and W. B. Lacina, Appl. Phys. Letters 18, 406 (1971).

3. R. G. Eguchi, W. H. Steier, M. M. Mann, and W. B. Lacina, 1971 IEEE/OSA Conference on Laser Engineering and Applications, Paper 17.9.

4. J. H. McCoy, Appl. Phys. Letters 15, 353 (1969).

5. D. E. Caddes, L. M. Osterink, R. Targ, Appl. Phys. Letters 12, 74 (1968).

6. O. R. Wood and S. E. Schwarz, Appl. Phys. Letters 12, 263 (1968).

7. T. J. Bridges and P. K. Cheo, Appl. Phys. Letters 14, 262 (1969).

8. S. Marcus and J. H. McCoy, Appl. Phys. Letters, 16, 11 (1970).

9. S. E. Harris and O. P. McDuff, IEEE J. Quantum Electronics QE-1, 245 (1965).

10. A. E. Siegman and D. J. Kuizenga, Appl. Phys. Letters 14, 181 (1969).

11. G. W. Hong and J. R. Whinnery, IEEE J. Quantum Electronics QE-5 367 (1969).

12. J. O. Hirschfelder, C. F. Curtiss, and R. B. Bird, Molecular Theory of Gases and Liquids, p 1110, John Wiley and Sons, Inc. New York (1954).

13. D. C. Smith and P. J. Berger, IEEE J. Quantum Electronics QE-7 174 (1971).

14. J. Gilbert and J. L. Lachambre, Appl. Phys. Letters 18, 187 (1971).

15. A. Nurmikko, T. A. DeTemple, and S. E. Schwarz, Appl. Phys. Letters 18, 130 (1971).

16. O. R. Wood, R. L. Abrams, and T. V. Bridges, Appl. Phys. Letters 17, 376 (1970).

17. A. J. Beaulieu, Appl. Phys. Letters 16, 504 (1970).

18. D. B. Cohn, K. R. MacKenzie, Phys. Rev. Letters, 28, 656 (1972).

19. J. B. Gerardo, J. T. Verdeyen, M. A. Gusinow, J. Appl. Phys. 36, 3526 (1965).

20. Liepmann and Roshko, "Elements of Gasdynamics," 1957, Wiley p 156.

21. A. K. LaFlamme, R. S. I. 41, 1578 (1970).

22. F. R. Nash, IEEE J. Quantum Electronics, QE-3 189 (1967).

23. T. Uchida and A. Ueki, IEEE J. Quantum Electronics, QE-3 17 (1967).

24. P. W. Smith, IEEE J. Quantum Electronics, QE-3, 627 (1967).

25. W. E. Lamb, Jr., Physical Review, 135 A 1420 (1964).

26. I. P. Kaminow, Applied Optics, 4, 123, (1965).

27. See for example, B. P. Lathi "Signals, Systems and Communications," Chapt. 11, John Wiley and Sons, Inc., New York (1965).

28. D. J. Kuizenga and A. E. Siegman, IEEE J. Quantum Electronics QE-6, 694 (1970).

29. A. E. Siegman and D. J. Kuizenga, IEEE J. Quantum Electronics, QE-6, 803 (1970).